REPORT DOCUMENTATION PAGE

Form Approved
OMB No. 0704-0188

1. AGENCY USE ONLY *(Leave blank)*	2. REPORT DATE	3. REPORT TYPE AND DATES COVERED
	11/9/98	Final - Sept. 94 - Sept. 98

4. TITLE AND SUBTITLE
In-Situ Nondestructive Examination of Weld Penetration

5. FUNDING NUMBERS
G-ONR-00149411088

6. AUTHOR(S)
Bryan A. Chin

7. PERFORMING ORGANIZATION NAMES(S) AND ADDRESS(ES)
Materials Engineering
Auburn University
201 Ross Hall
Auburn, AL 36849

8. PERFORMING ORGANIZATION REPORT NUMBER

9. SPONSORING / MONITORING AGENCY NAMES(S) AND ADDRESS(ES)
Office of Naval Research
Program Officer George R. Yoder ONR 332
Ballston Centre Tower One
800 North Quincy Street / Arlington, VA 22217-5660

10. SPONSORING / MONITORING AGENCY REPORT NUMBER

11. SUPPLEMENTARY NOTES

a. DISTRIBUTION / AVAILABILITY STATEMENT

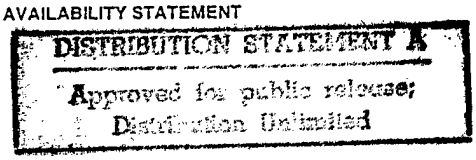

12. DISTRIBUTION CODE

19981120 020

13. ABSTRACT *(Maximum 200 words)*

The objective of this program is to develop infrared sensing techniques to monitor and control welding penetration in gas tungsten arc and submerged arc welding processes used by the US Navy in the construction of ships. The infrared sensor will provide in-situ, nondestructive weld quality information that can be used to correct depth of penetration prior to solidification of the molten metal pool. In this project the changes in surface thermal distributions resulting from intentionally induced perturbations during the welding process were measured using a low cost infrared sensor. This information was compared with the predictions of heat transfer calculations. A control system was constructed which utilizes the results of the predictions to model and control the weld penetration process. The ability to prevent plate burnthrough for variable gap and plate thickness variations was demonstrated.

14. SUBJECT TERMS	15. NUMBER OF PAGES
Welding, Infrared Sensors, Control, Penetration	68
	16. PRICE CODE

17. SECURITY CLASSIFICATION OF REPORT	18. SECURITY CLASSIFICATION OF THIS PAGE	19. SECURITY CLASSIFICATION OF ABSTRACT	20. LIMITATION OF ABSTRACT
Unclassified	Unclassified	Unclassified	UL

FINAL REPORT

IN-SITU NONDESTRUCTIVE EXAMINATION OF WELD PENETRATION

Bryan A. Chin
Auburn University, AL 36830
November 9, 1998

Grant # ONR-00149411088

TABLE OF CONTENTS

I. INTRODUCTION

The fabrication, construction and repair of modern structures require precise manufacturing, assembly and joining of components. Increased competition and highly engineered designs with stringent quality requirements have necessitated improved productivity and modernization of manufacturing processes. In industries like shipbuilding, pressure vessel fabrication, power generating systems, etc.; automation of the welding process to obtain optimal performance through improved weld properties and joint reliabilities at no increase in cost has become imperative. Despite a concentrated quality control program, weld reliability and repeatability continues to be a factor limiting the performance of many fabricated parts. The non-destructive testing, identification and repair of weld defects run as high as 25% of the total weld production costs and is a major contributor to lengthy fabrication and construction time.

The intense heat and fumes generated by the welding process along with early eye fatigue caused by the brilliance of the arc and environments with restricted access, limit the human operator to short periods of quality welding. The average industrial arc welding time, time in which the arc is struck is approximately 35-40% due to the above reasons. Hence the welding process is one manufacturing task in which productivity and quality can be greatly improved by the application of advanced sensing techniques, artificial intelligence and robotics.

Semi-automatic welding systems rely on the skill of the welding operator to ensure high integrity welds. Preset automated systems, in which the welding parameters are pre-programmed before any welding takes place, lack the ability to compensate for perturbations, which arise during the welding process. Perturbations are caused due to thermally induced distortions, improper joint preparation and fit-up, changes in materials composition, changes in shielding gas composition and sudden changes in plate thickness, resulting in torch offset, non-uniform penetration and lack of side wall fusion.

To be able to weld successfully in conditions where the weld parameters cannot be totally defined requires a system capable of sensing the variations and modifying some aspects of the machine behavior sufficiently to allow it to cope with these perturbations in real-time. Hence the

need for systems which can monitor and control the in-process status of the welding process, i.e., systems incorporating joint seam tracking and adaptive process control. Benefits include enhanced, consistent and continuous welds, reduced after-the-fact non-destructive testing and repair, opportunity to increase welding speed and deposition rate to the technological limit of the process and ability to perform difficult and dangerous tasks that would not be possible otherwise, for example remote weld repairs in radioactive environments.

Sensing and control of the submerged arc welding process using point infrared sensing technique was studied. A model of heat exchange between point infrared detector and weldment surface was established to study the detector response under different conditions. A submerged arc welding process feedback control system was integrated. Plates with different configurations were welded using the developed control system to test the performance. Results of the experiments are presented in this report.

OBJECTIVE

The objective of this project is to develop a low cost, real-time monitoring and control of weld penetration using infrared sensing to eliminate or mitigate defects such as burn through, improper weld penetration, lack of side wall fusion and slag inclusions which occur due to thermal distortion, improper fit-up and joint gaps, and to reduce the welding costs and time through the elimination of the use of backing materials.

II. BACKGROUND

Significant advances have been made in the last decade in the development of automatic welding systems. An essential element of any monitoring and control system is the sensor, which observes and/or measures the performance of the process by monitoring one or more variables. This information serves as the feedback signal for the implementation of the control system. Several sensing techniques have been developed for measuring the penetration depth during the welding process. They can be classified as either direct measurement or indirect measurement techniques. Most of the techniques do not allow the direct measurement of the weld penetration depth since it is not visible from the surface of the plate. This requires the measurement of a physical weld characteristic, which is related to the penetration depth. An example of the direct measurement technique is the ultrasonic sensing method. Examples of the indirect method include oscillating/rotating arcs; weld pool oscillation frequency; optical (laser/photo-diode, laser/solid state camera); X-ray and infrared.

Ultrasonic Method

This method allows the direct measurement of the geometry of the weld pool. Both contact and non-contact methods have been investigated for monitoring the depth of penetration during welding. Normal beam and angle beam pulse echo methods have been used to locate weld defects such as porosity, inclusions, improper penetration and lack of sidewall fusion. The angled beam method has been found to be more advantageous since it allows the topside placement of the transducer. Hardt and Katz [1] conducted one of the first feasibility studies into the application of ultrasonic sensing techniques. A relationship between the radius of a stationary weld pool and the time-of-flight of the return signals was developed using normal beam pulse-echo method. Researchers at Idaho National Engineering Laboratory performed feasibility studies on the use of ultrasonic transducers adjacent to a moving weld pool. Carlson et al investigated the use of shear waves [2] and longitudinal waves [3] to determine the weld bead geometry and discontinuities during welding. The ultrasonic transducer was either

mounted onto a rubber wheel which traversed the weld with the welding torch or the transducer was held in contact with the plate using springs. The non-contact ultrasonic sensing method has also been investigated by the same team [4]. In this method, laser and electromagnetic-acoustic transducers (EMAT) were employed to generate and detect the acoustic waves respectively. In this method, the acoustic waves generated in the plate by the use of high-energy lasers were detected using a permanent magnet, which generated a magnetic field in the weldment. The acoustic waves caused the charges to move thereby generating a secondary field, which was detected by a pickup coil. Unfortunately the EMAT system had very low signal-to-noise ratio. The laser also produced some surface damage along the weld.

Fenn [5] developed a closed-loop penetration control system utilizing ultrasonic sensors. Two angle-beam piezoelectric transducers were mounted in line with the welding electrode and used to measure weld pool penetration during the welding process. These measurements were utilized by a feedback controller to maintain a constant penetration depth during the submerged arc welding process.

The major difficulties with the ultrasonic sensing techniques were the effects of both the temperature and the temperature gradient on the ultrasonic signals generated. The high temperatures attenuated the signal resulting in low signal-to-noise ratio, which in turn caused serious difficulties in the interpretation of the ultrasonic signals. The large temperature gradients caused the signals to shift in the time domain due to the strong temperature dependence of the speed of sound in the material. Additional problems such as the requirement of contact of the transducer with the plate, contamination of weld with the couplant, and false signals due to loss of contact or variable surface condition prevented the implementation of this technique on the shop floor.

Weld Pool Oscillation Method

The formation of ripples on the surface of gas tungsten arc spot welds were recognized to be caused by naturally occurring oscillations excited by the arc jet plasma force. Experimental studies [6] showed that normal-mode weld pool vibrations were related to the pool geometry for stationary, full penetration welds. Higher order modes of oscillation were observed for partially

penetrated welds and for the case of traveling arc. One favorable effect of the pool vibration, in relation to sensing, is its effect on the arc voltage. Pool oscillations cause the arc length to vary thus causing the arc voltage to fluctuate. The weld pool oscillation frequency can be revealed by proper signal processing of the measured arc voltage. Renwick and Richardson [7] developed an empirical relationship between the observed voltage variations and the weld pool geometry for stationary, partially penetrated welds. Further experiments have indicated that the width of the weld pool was the most important factor influencing the pool oscillation frequency. Xiao and den Ouden [8] observed a distinct transition in the modes of oscillation between partially penetrated welds and fully penetrated welds for both stationary and traveling arc. Madigan et al [9] have investigated the use of the weld pool oscillation technique for monitoring and controlling the GTA welding process by measuring the arc voltage variations. But the oscillation frequencies for partial and full penetration welds were found to overlap, leading to false signals and resulting in improper control. The control system was also found to breakdown for shallow welds.

Optical Sensing Methods

In the optical sensing methods, attempts are made to convey to the controller what the human eye sees during the welding process. Most of the optical sensing methods developed have involved the use of laser/solid state camera combination or the laser/photo-diode combination for seam tracking and weld geometry control. In one of the early optical sensing techniques [10], a series of photo-diodes were used for measuring either the front face weld bead width or the backside light intensity. The measurements were then empirically related to the weld penetration depth. In the other method, a solid state camera views the illuminated stripe produced by the laser on the weld joint. The joint tracking and weld geometry controls were achieved using optical triangulation mathematics and image processing. Kovacevic et al [11] have developed a system for monitoring the weld geometry using laser stripping and a high shutter speed camera. Richardson et al [12] have investigated the use of coaxially aligned viewing optics for monitoring GMAW and GTAW processes. In both of the above cases, image processing was used to extract the weld pool size and the joint configuration.

Unfortunately smoke, spatter and the arc itself affect these systems. The hardware is fragile, costly, intrusive and requires sophisticated image processing. This method is not feasible for monitoring the SAW process since the weld pool is covered by flux. Moreover, the empirical relationship between the weld pool width and the penetration depth begins to fail under dynamic conditions resulting in improper control of the weld parameters.

Radiographic Sensing Methods

Rokhlin and Guu [13] have investigated the use of radiography for monitoring and control of penetration. Real-time radiographic images were acquired and processed using digital image processing software and used for closed loop control of the welding parameters. The darkness (density) of the image was used to indicate the depth of penetration. However, the location of the image that was observed for controlling the weld was about 25mm behind the electrode in order to avoid the noisy weld pool region. Unfortunately, this delayed the control action and the system failed to achieve adequate control under actual shop floor conditions. In addition, access to both sides of the weldment is necessary to accommodate the bulky x-ray source and an image intensifier. Extensive safety procedures required for protection from the x-rays make this technique impractical for shop floor applications.

Infrared Sensing Techniques

All materials above 0 Kelvin emit infrared radiation and the radiation intensity is a function of the temperature. Kirchhoff defined the activity of the electromagnetic spectrum and developed quantitative data and equations to identify IR energy. The IR part of the electromagnetic spectrum spans wavelengths from 0.7 to 1000 microns. The band between 0.7 to 20 microns is used for practical temperature measurements. Planck [14] derived the theoretical relationship between spectral emissivity, temperature and the radiant energy (fig.1). The IR radiation energy is converted into electrical energy using IR detectors. The electrical signal from the detector can be displayed in units of temperature as in infrared pyrometers or processed and used for monitoring and controlling applications.

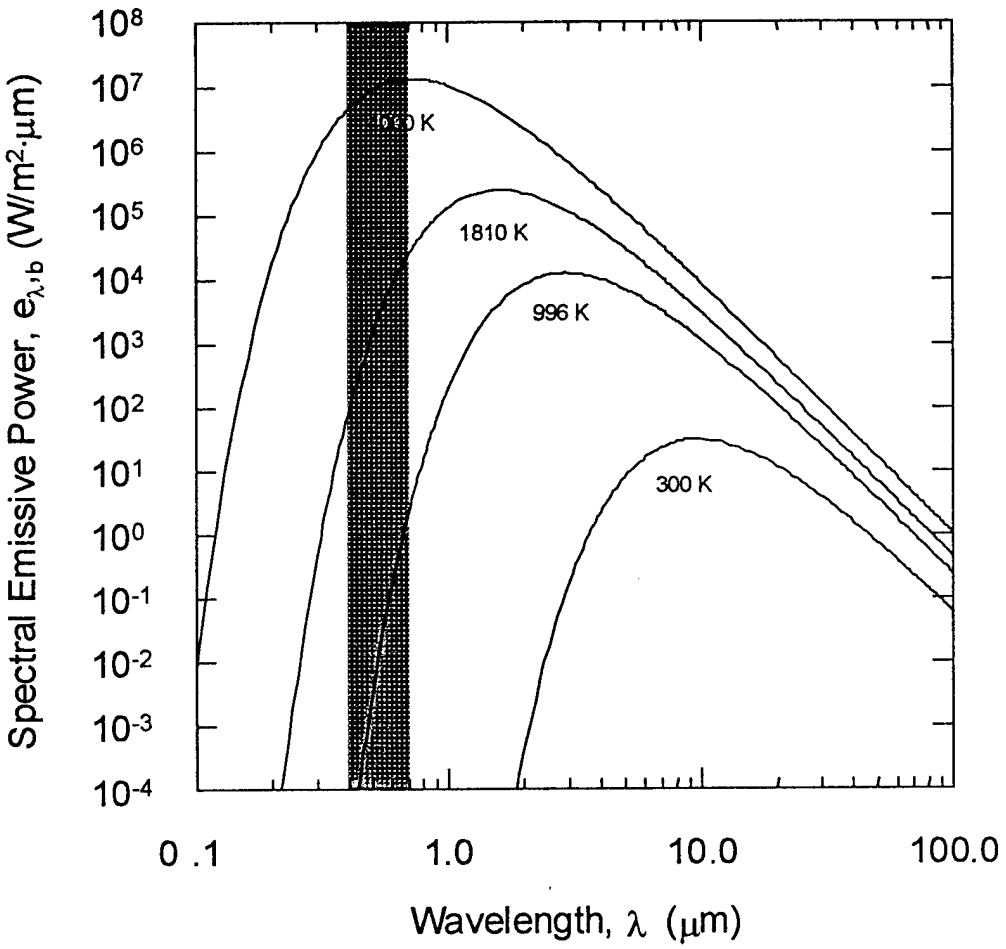

Figure 1. Planck's spectral distribution for a blackbody. Plotted temperatures represent the approximate temperature of the welding arc (4000 K), the melting point of pure iron (1810 K), the eutectoid temperature from the Fe-C phase diagram (996 K) and room temperature (300 K). The shaded areas correspond to the visible spectrum (0.4-0.7 μm), the bandwidth of the Inframetrics 525 camera (8-12 μm) and the bandwidth of the point IR sensor (8-14 μm).

The temperature distribution around the weld pool provides important information on the status of the welding process. The pool shape, absolute temperature and symmetry of temperature distribution are directly related to several welding process variables such as joint mismatch, root gap variations, plate thickness, composition, etc., of the plates. Temperature monitoring near the weld pool by IR sensor is very convenient since physical contact with the surface is not required. IR detectors are simple, have fast response times, and are easier to adapt to the shop floor conditions.

Infrared sensing techniques have been utilized to study the various aspects of the weld as early as the 1960s. Infrared cameras, point sensors, and other variations have been used for measuring the temperature distribution around the weld pool, for seam tracking, bead width control and penetration control. Much of the work involving infrared sensing for weld process control has taken place at Auburn University. A feasibility study conducted by Chin et al [15] using thermographic infrared camera has shown that various disturbances to the welding process produce tell tale signatures in the surface temperature fields of the parts being welded. The infrared thermography equipment consisted of single waveband (8-12 microns) infrared detector, image processing system with isothermal line scan, area scan and color monitor. The instrument was capable of measuring -20^{0}C to 2500^{0}C with a manufacturer claimed resolution of $\pm$0.2 ^{0}C. Figure 2 shows a picture of the area scan and line scan of a weld pool. Figure 3 shows the effect of joint mismatch on the distribution of the surface isotherms. Based upon this work, several seam tracking and penetration control schemes have been developed. Nagarajan and Chen [16] have implemented a control strategy based upon the size and area enclosed by the surface isotherms for GTAW and GMAW processes. The isotherm radii were used to identify the arc position relative to the joint. It was found that the minor axes and area of the ellipse of isotherms are the most sensitive variables to study changes due to the variations in the penetration depth and thickness of the plate being welded. Wang [17] proposed a control strategy based on the width and height of a line scan through the molten weld pool.

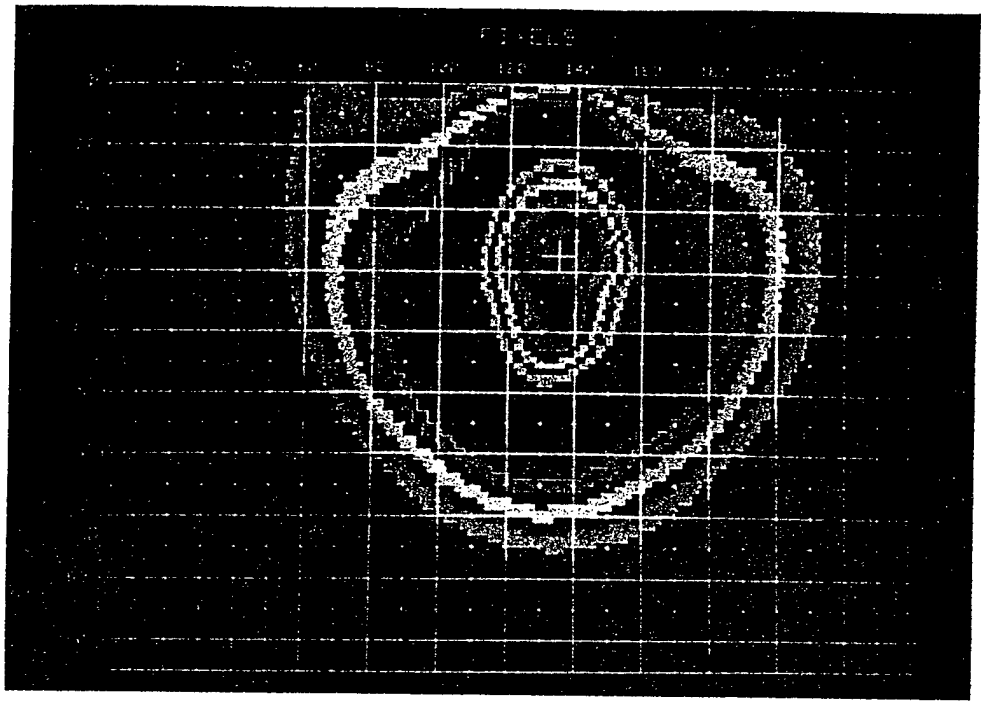

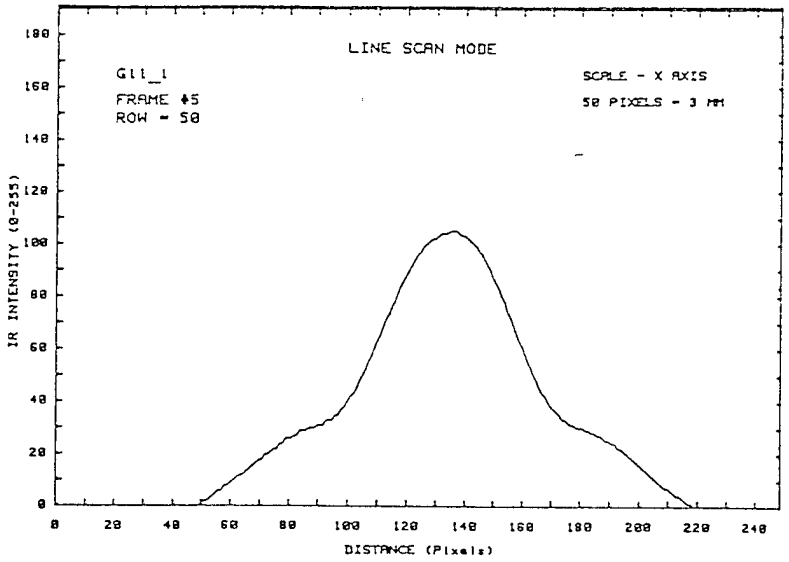

Figure 2. Area scan and line scan of the weld pool.

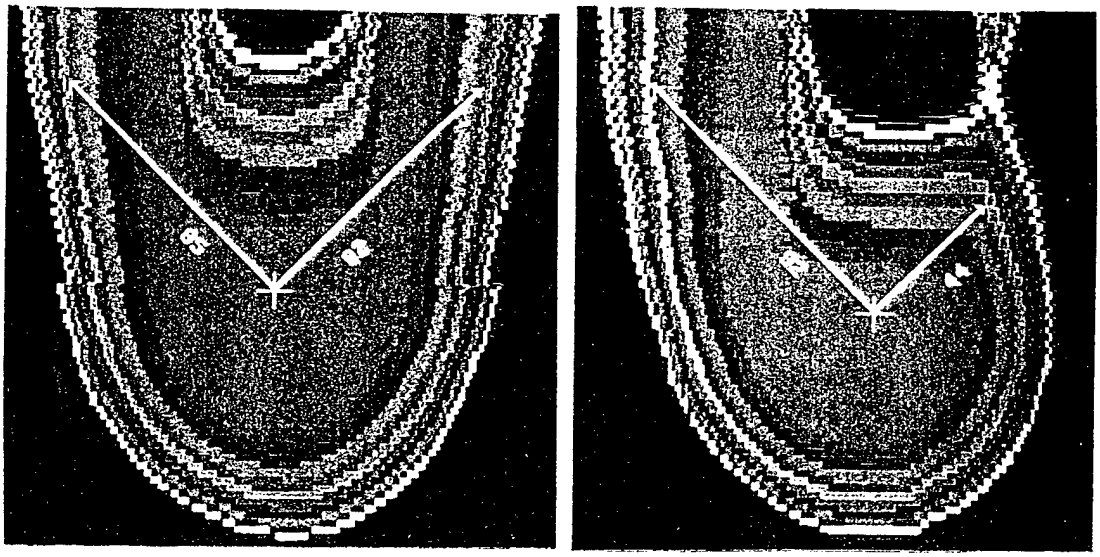

Figure 3. Effect of joint mismatch on the distribution of the surface isotherms.

In an extension to this idea, Banerjee [18] has implemented a penetration control system for the GTAW process based upon the thermal gradient across the weld pool. Doumanidis [19] developed a system, which controlled the weld bead geometry and HAZ cooling rates using infrared thermal profile measurements. Brown [20] used the infrared camera system to monitor resistance spot welds and detect the weld nugget and its quality. A relationship was established between the isotherm geometry, weld joint strength and weld nugget size.

Unfortunately, infrared cameras are costly, fragile, intrusive and require complicated image processing to extract the necessary information. Most of the systems developed have been for either GTAW or GMAW processes. Not much work has been done to investigate the use of an infrared control system for the SAW process, which is widely used in shipbuilding, pressure vessels and other heavy manufacturing industries.

An inexpensive alternative to the infrared camera is the point infrared sensor, which is also easy to use and least intrusive. Ramsey et al [21] conducted the first feasibility study of using the point infrared sensor for monitoring the temperature distribution around the weld pool. One of the earliest attempts to employ a point infrared sensor for the measurement of penetration depth was reported by Smith [10] in which backside emissions were monitored. Recent work has focused on the use of thermopile infrared detectors as a topside-sensing device. Point infrared sensors have been used for monitoring and control of GTAW and SAW processes [22, 23].

III. INFRARED SENSOR DEVELOPMENT

Various infrared sensors have been used to measure the surface temperature distribution during arc welding. Most infrared sensors used to date to monitor the welding process are scanning infrared cameras. High initial cost, delicate optical and transmission components, and arc interference have contributed to the slow implementation of this type of sensors. Recent advances in infrared detector technology however, have brought about low cost, rugged devices which are not as susceptible to arc radiation effects. Replacement of expensive infrared cameras with low cost, rugged sensors will greatly promote the implementation of this technology in metal fabrication industries.

Development of a point infrared sensor was undertaken in an effort to reduce the size and cost of the sensing system. The developed sensor must also be able to stand the harsh conditions surrounding the welding arc without affecting the sensor performance. The physical size of commercially available units is too large to allow placement of sensors in close proximity to the welding arc and the cost is usually high. In order to overcome these limitations, a point infrared sensor was designed and constructed. The IR detector used in this work is a thin film thermopile with an active area of $4X10^{-2}$ cm^2 and 48 hot junctions. The detector has a germanium window, which is transparent to radiation in the 8-14 μm wavelengths. The response time constant is approximately 50-100 msec and the sensor generates 5100 μV dc output at 10 mW/cm^2 IR incident radiation. The thin film is enclosed in a metal container filled with xenon gas. The detector generates an emf based on the radiant energy reaching it. The output emf is also a function of the temperature difference between the target and the detector itself. The voltage generated by the detector V_{det} can be expressed as follows,

$$V_{det} = M (T_T^4 - T_D^4) \quad (1)$$

where, T_T is the target temperature (K)

T_D is the detector case temperature (K) and

M is a constant, which depends on the area of the target, area of the detector, distance from the object to detector and the responsivity of the detector.

Under this project, the uncooled IR detector was designed for optimum measurement of IR radiation in the long wave length range (>5 μm). One hundred prototype detectors were fabricated using thin film technology. Of these one hundred detectors, approximately 30% performed as anticipated with specifications meeting or exceeding design specifications.

Background

An analysis of the radiative exchange of heat between two surfaces was performed in an effort to predict the performance of the custom built infrared sensor. The following assumptions were employed throughout the analysis:

- All surfaces were treated as blackbodies; diffuse emitters, emissivity of unity.
- Constant temperature over all designated surfaces.
- Absorption by all materials in the optical path was neglected.

The notation of Siegel [24] was used in this analysis.

Referring to figure (4), the rate at which energy dq leaves a differential surface dA_1 and is incident upon differential surface dA_2 is given by

$$dq_{d_1 \to d_2} = i'_{b,1} dA_1 \cos\theta_1 d\omega_1 \tag{2}$$

where, $d\omega_1$ is the solid angle subtended by dA_2 when viewed from a point on dA_1

$$d\omega_1 = \frac{dA_2 \cos\theta_2}{S^2} \tag{3}$$

The blackbody radiant intensity $i'_{b,1}$, is found by integrating Planck's spectral distribution of emissive power by a blackbody, over all wavelengths to give the

Table 1. Symbol definitions used in net heat exchange analysis.

Symbol	Definition	Units
i'_b	blackbody radiant intensity	W/m^2·sr
λ	Wavelength	μm
T	Temperature	K
A	surface area	m^2
S	distance between two points	M
L	target distance, separation distance	M
D	Diameter	M
R	radial distance	M
N	surface normal vector	
σ	Stefan-Boltzmann Constant	5.67·10^{-8} W/m^2·K^4
C_1	first radiation constant	3.742·10^8 W·μm^4/m^2
C_2	second radiation constant	1.439·10^4 μm·K
R	detector responsivity	10-25 V/W
V_{det}	detector output voltage	V

$$e_{\lambda b}(\lambda) = \pi i'_{\lambda b} = \frac{2\pi C_1}{\lambda^5 (e^{C_2/\lambda T}) - 1)} \tag{4}$$

familiar Stefan-Boltzmann law for the total hemispherical emissive power

$$e_b = \pi i'_b = \int_0^\infty e_{\lambda b}(\lambda) d\lambda = \sigma T^4 \tag{5}$$

Rearranging and substituting Equations 3 and 5 into Equation 2 gives the following equation for the rate at which energy leaves dA_1 and is incident upon dA_2.

$$dq_{d_1 \to d_2} = \frac{dA_1 \cos\theta_1 dA_2 \cos\theta_2}{\pi S^2} \sigma T_1^4 \tag{6}$$

The total amount of energy per unit time that leaves surface A_1 and is incident upon A_2 is found by integrating Equation 6 over the two surfaces

$$q_{1\to 2} = \sigma T_1^4 \int_{A_2} \int_{A_1} \frac{\cos\theta_1 \cos\theta_2}{\pi S^2} dA_1 dA_2 \tag{7}$$

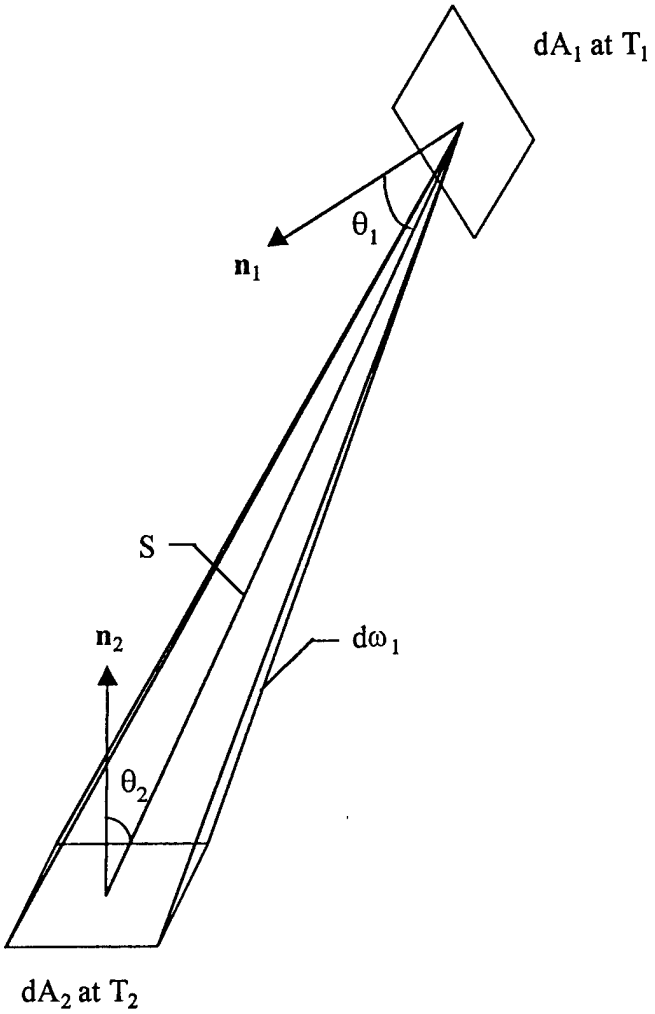

Figure 4. Radiative exchange between two differential surface area elements.

The integrand in Equation 7 is solely a function of the geometry of the situation. A view factor, $dF_{d_1\text{-}d_2}$, which takes into account the geometry of the configuration, can be defined as the fraction of the radiation leaving surface dA_1 that is incident upon surface dA_2. This is expressed as

$$dF_{d_1-d_2} = \frac{dq_{d_1\to d_2}}{dq_{d_1}} = \frac{\cos\theta_1 \cos\theta_2}{\pi S^2} dA_2 \tag{8}$$

An integrated view factor can also be defined that is the fraction of the total radiation leaving surface A_1 that is incident upon surface A_2 is given by

$$F_{1-2} = \frac{q_{1\to 2}}{q_1} = \frac{1}{A_1} \int_{A_2}\int_{A_1} \frac{\cos\theta_1 \cos\theta_2}{\pi S^2} dA_1 dA_2 \tag{9}$$

so that the total rate at which energy leaves surface A_1 and is incident upon A_2 can be written as

$$q_{1\to 2} = A_1 F_{1-2} \sigma T_1^4 \tag{10}$$

The above general derivation was for an arbitrary geometry. For complex geometries the double integral can be difficult to integrate. The arrangement used in actual welding experiments could be approximated by the simple geometry of the exchange between a differential element and a finite circular area. A circular disk of diameter A_1 exchanges radiation with a differential area dA_2 where A_1 would correspond to the weldment and dA_2 would correspond to the sensing element. The double integral can be simplified by noting that the total energy radiated from dA_2 is given by

$$q_{d_2} = dq_{d_2} = \sigma T_2^4 dA_2 \tag{11}$$

and the relevant view factor is

$$F_{d_2-1} = \int_{A_1} dF_{d_2-d_1} = \int_{A_1} \frac{dq_{d_2\to d_1}}{dq_{d_2}} = \int_{A_1} \frac{\cos\theta_1 \cos\theta_2}{\pi S^2} dA_1 \tag{12}$$

With the aid of the geometry shown in figure 5, the last integral of Equation 12 can be evaluated to give

$$F_{d_2-1} = 2L^2 \int_0^{D/2} \frac{r}{(r^2+L^2)^2} dr = \frac{D^2}{D^2+4L^2} \tag{13}$$

so that the total rate at which energy leaves dA_2 and is incident upon A_1 is

$$q_{d_2 \to 1} = dA_2 F_{d_2-1} \sigma T_2^4 \tag{14}$$

To determine the total energy leaving A_1 that is incident upon surface dA_2, the view factor reciprocity relationship, given by Equation 15, can be used to determine the second view factor, $dF_{1\text{-}d_2}$

$$dA_2 F_{d_2-1} = A_1 dF_{1-d_2} \tag{15}$$

The net exchange of heat between A_1 and dA_2 is then the difference in the total energy transfered from one surface to the other,

$$q_{1 \Leftrightarrow d_2} = q_{1 \to d_2} - q_{d_2 \to 1} \tag{16}$$

This gives for the total heat exchange between surface A_1 and dA_2

$$q_{1 \Leftrightarrow d_2} = A_1 dF_{1-d_2} \sigma \left(T_1^4 - T_2^4\right) \tag{17}$$

This expression allows the approximation of the net energy exchange between the target surface and the detector. Each term on the right side of Equation 17 can now be calculated from either the geometry of the situation or a welding heat transfer model.

A responsivity coefficient R is specified by the infrared detector manufacturer that allows one to calculate the voltage output of the sensor from the knowledge of the net heat exchange. Modifying Equation 17 gives

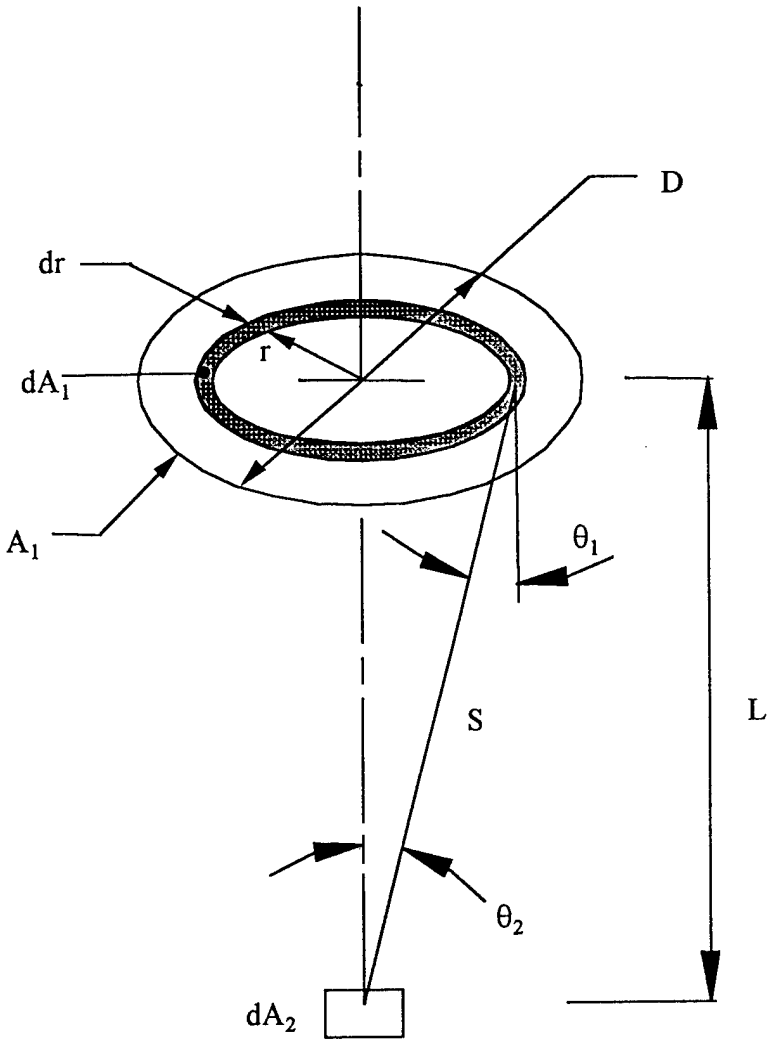

Figure 5. Geometry for view factor, $F_{d_2\text{-}1}$, calculation between a differential area d_2 and a circular surface of area A_1.

$$V_{det} = A_1 dF_{1-d_2} \sigma \left(T_1^4 - T_2^4\right) R \tag{18}$$

Further modifications could be made to include the emissivities of the two surfaces, the absorption of the energy by the optical window and the bandwidth of the thermopile sensor. These modifications were not included in the above analysis in order to reduce the reliance upon unknown empirical coefficients. These modifications would serve only as scaling factors in the final analysis. The above analysis however, still provides useful insight into the response of the detector as will be shown in the following discussion.

Modeling

The above analysis provides a first approximation to the heat exchange between the plate surface and the sensor. One of the conditions of this analysis is that a constant temperature exists throughout the area of interest. As can be seen from a solution to the convection-diffusion equation, figure 6, steep temperature gradients exist in the vicinity of the welding arc. The assumption of constant temperature throughout the field-of-view (FOV) of the sensor is not very reasonable. Combining the results of the above derivation and a solution to the convection-diffusion equation, a finer approximation to the net heat exchange between the plate surface and the sensor can be calculated. The results of these calculations were used to investigate the response of the point infrared sensor as a function of its placement about the welding arc.

When the sensing element is placed parallel to its target's surface, the FOV projected by the sensor sweeps out a circular area on the surface. A polar mesh was generated, as in figure 7 that would occupy the FOV of the sensor and would lie in the calculation domain. The overall size of the polar mesh was made to match the FOV of the sensor. The density of the mesh, the number of nodes and nodal spacing, could be adjusted in the computer program. The temperatures at the nodes in the polar mesh were interpolated from the nodal temperatures previously calculated with the heat transfer model.

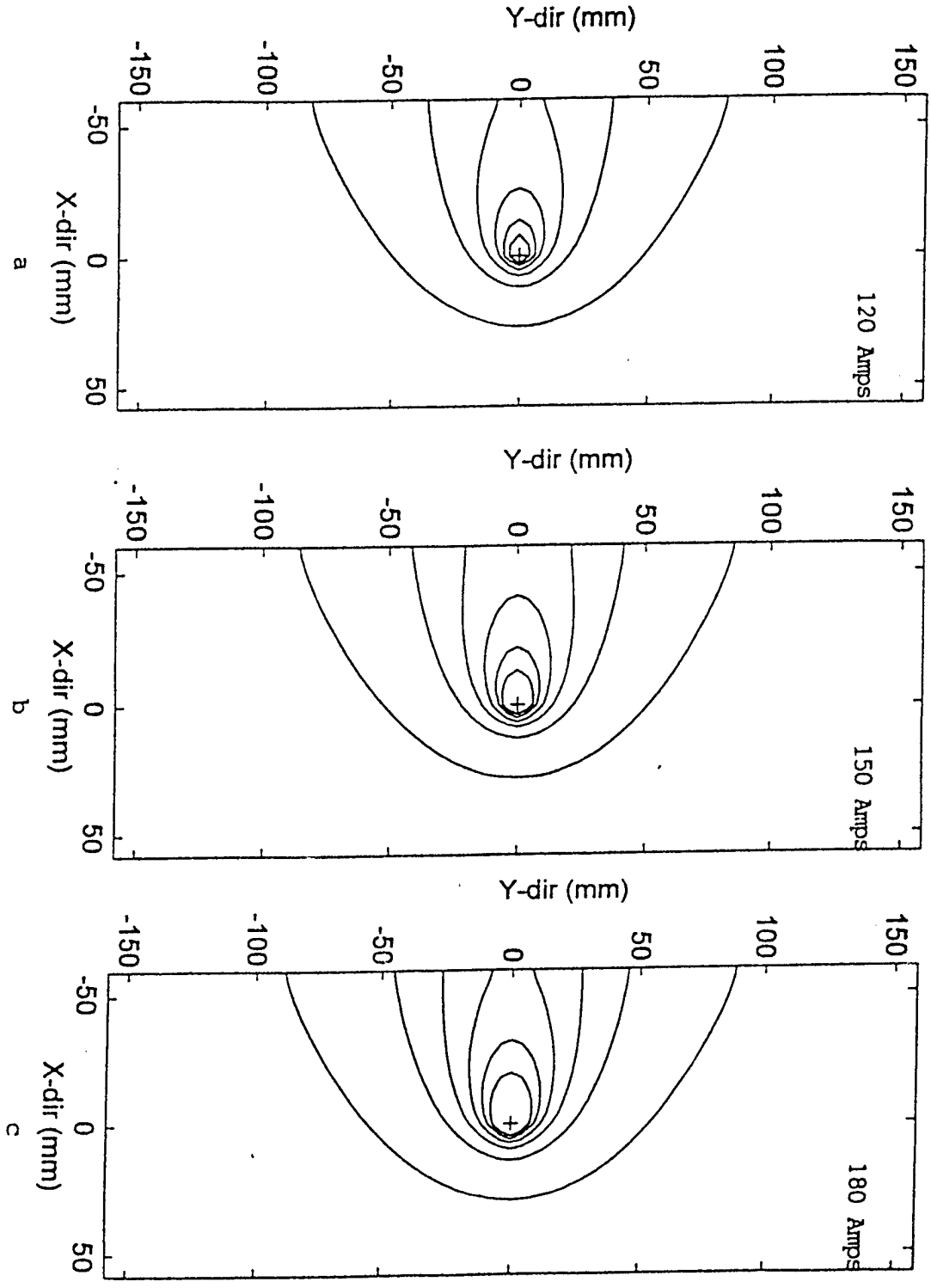

Figure 6. Steady-state solution for welding heat inputs of 2.4, 3.0 and 3.6 kW

The position of the polar mesh on the plate surface was varied as a function of radial distance from the arc center and as angular displacement from the welding direction. The sensor surface was centered directly over the polar mesh at a specified height. The overall size of the polar mesh was a function of the distance between the sensing element surface and the weldment surface and was calculated using Equation 25 presented later in this chapter.

The view factor, $dF_{d_1\text{-}d_2}$, was calculated for each node within the polar mesh using Equation 8. The temperature was assumed constant over the area element in which the node was located. Then the net heat exchange between each of the elements, $q_{d_1\text{-}d_2}$, in the polar mesh and the sensor was calculated using Equation 6. The total heat reaching the sensor element, $q_{1\text{-}d_2}$, was then just the sum of all of the individual elemental net heat exchanges. The net heat exchange was calculated for both steady state and transient cases.

The overall size of the polar mesh must still be determined. The field of view of the sensor depends upon the mechanical geometry of the sensor. In a following section, the mechanical design of the sensor will be described. The results of the calculations to estimate the net heat exchange are presented in the discussion section of this chapter.

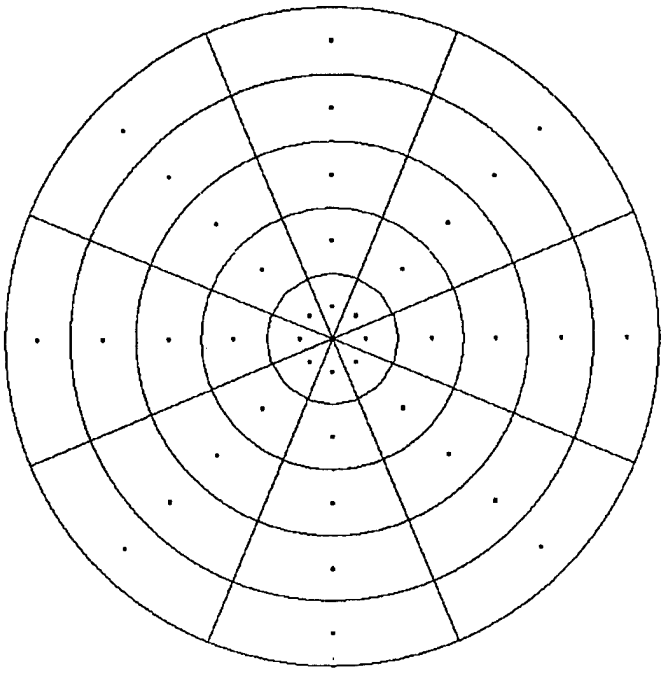

Figure 7. Example of a polar mesh that was generated to occupy the field of view of the IR sensor. The temperature of each node was interpolated from a solution to the convection-diffusion equation.

Circuit design and analysis

Signal conditioning circuitry was designed to process the raw detector signal before it was utilized. The sensor electronic system consisted of two major components, a sensor head and a signal conditioner. The sensing head was intended to be placed as close as possible to the welding arc and contain a minimal number of electronic components. The purpose of the sensing head was to amplify the thermopile detector signal above the background electrical noise. The signal conditioner was located away from the welding arc where environmental considerations were not a factor. The purpose of the signal conditioner was to provide further amplification and filtration of the detector signal before being passed on to the data acquisition system. A description of the circuitry follows.

The main component of the sensor was a thermopile detector. The detector was packaged in a T0-5 canister, backfilled with xenon gas. A germanium window (8-14μm) was in place to allow the infrared radiation to reach the sensing element and to serve as a filter against unwanted wavelengths of radiation. The sensing element within the detector was a 2 mm square thin film with 48 hot junctions connected in series. The detector functioned by self-generating an electric potential in proportion to net exchange of radiation between the detector and its target.

In the first section of the signal conditioning system, the sensing head, the thermopile detector output signal was amplified with an instrumentation amplifier using a configuration as shown in figure 8. This circuit was implemented with a single instrumentation amplifier (Analog Devices AD524). Amplification of the detector output was necessary due to the presence of electrical noise in the vicinity of the welding arc. Signal gains of 10, 100, or 1000 could be chosen by the position of a jumper on the sensing head circuit board. A gain of 100 was found to give adequate amplification of the thermopile voltage from the sensing head to the signal conditioner without saturating the amplifier output during measurement. This gives the output of the sensing head as

$$V_0 = 100 V_{\text{det}} \tag{19}$$

The signal processor was located away from the welding arc and consisted of three separate stages: 1) offset 2) filter and 3) gain. Through the combined adjustment of the signal gain and offset, the sensor signal could be optimized for the data acquisition system, thus improving the overall sensitivity of the welding process control system. Filtration of the sensor signal was necessary due to presence of undesirable electrical noise in the welding environment. While gain is seen as the final stage of the signal conditioning circuit, in fact each stage contributed to the overall system gain. The electrical circuit design for the signal processor is shown in figure 9 and will be described below. The four op-amps were implemented with a single quad op-amp (Analog Devices AD713).

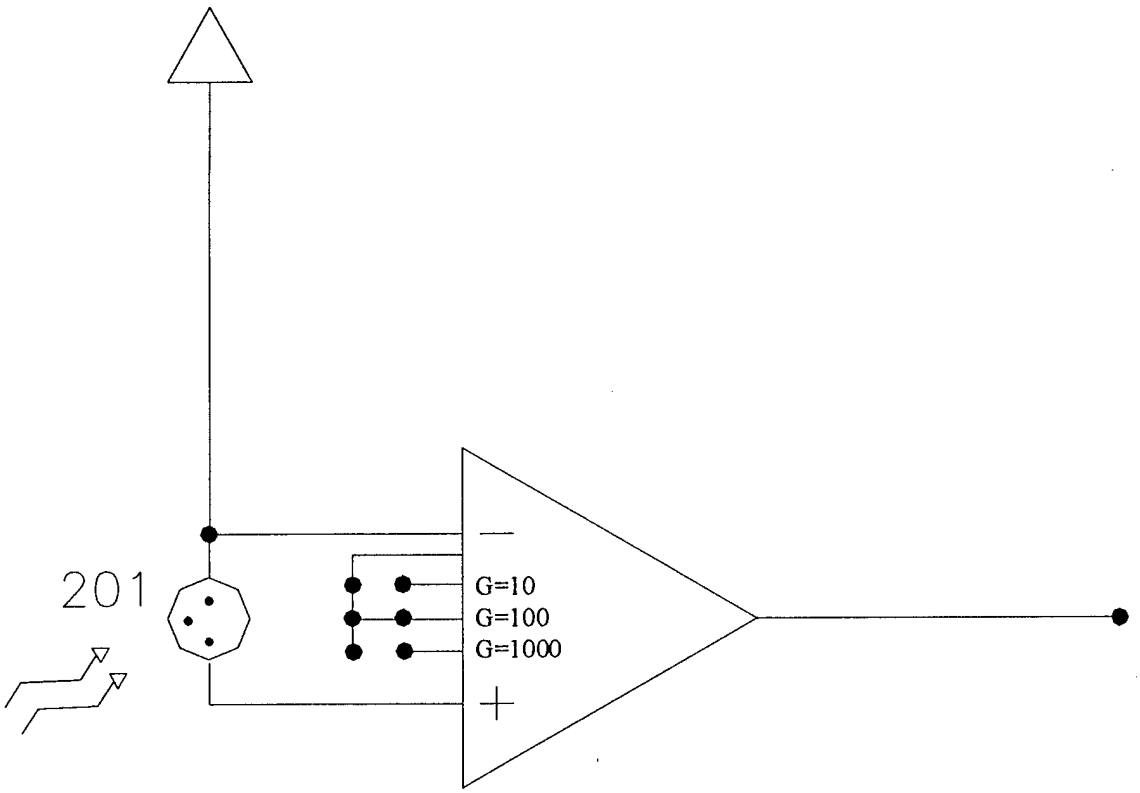

Figure 8. Circuit diagram of sensing head circuitry. Infrared radiation excites the thermopile detector. An instrumentation amplifier amplifies the thermopile signal by a switch selectable gain.

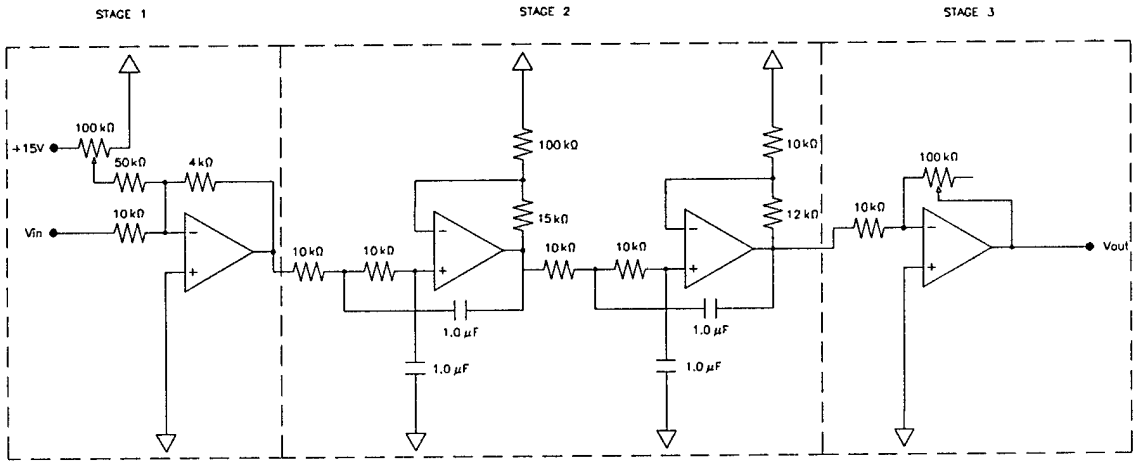

Figure 9. Circuit diagram for infrared signal conditioning unit. Circuit divided into 3 stages, 1) offset, 2) filter and 3) gain.

The first stage (offset) of the signal conditioning unit was based on a simple addition circuit using a single op-amp. A voltage divider, built with a 10-turn potentiometer and the power supply voltage, was used to provide the second input to this stage, the first input being the sensor signal. The output of this stage is described by the following equation.

$$V_1 = -\frac{1}{25}(3n_o + 10V_0) \tag{20}$$

where V_1 is the output of the first stage of the signal processing unit, V_0 is the input from the sensing head and n_o is the number of turns on the external potentiometer for offset adjustment. With the external potentiometer at zero turns, a gain of 1/2.5 would be in effect at the output of this stage. This minimum gain value was chosen to eliminate the gain in the following filter stage in order to keep the signal from saturating.

The second stage (filter) consisted of a four-pole, low-pass Butterworth filter that was used to smooth the signal from the sensor head. This filter was designed with a cutoff frequency of 15 Hz, well below the AC line frequency of 60 Hz. The overall gain of this stage was fixed and is given by:

$$V_2 = 2.5 \cdot V_1 \tag{21}$$

where V_2 is the output of the second stage and V_1 is the input from the first stage.

The third stage (gain) was based on a simple inverting amplifier design. A 10-turn potentiometer was used to establish the gain at this stage. For each turn of the pot, the gain increased by one as can be seen in the following equation:

$$V_3 = -n_g \cdot V_2 \tag{22}$$

where V_3 is the output of the third stage, V_2 is the input from the second stage and n_g is the number of turns on the external potentiometer for gain adjustment.

The overall effect of each of the stages on the final output of the sensor processing unit is given by the following equation:

$$V_3 = n_g \cdot (0.3n_o + 100V_{det}) \tag{23}$$

Mechanical Design and Analysis

As can be seen from Equation 17, the thermopile detector is sensitive not only to its target's temperature but also to the temperature of the detector itself. Due to the intense heat surrounding the welding arc, the sensor head was housed in a copper cooling jacket. The cooling jacket consisted of two concentric copper tubes with two additional smaller copper tubes brazed to the outer tube to serve as inlet and outlet ports for the coolant. A photograph of the cooling jacket is shown in figure 10. A mechanical drawing and dimensions of the cooling jacket is shown in figure 11. The TO-5 container for the thermopile detector was placed in the cooling jacket where it was held in physical contact with the copper tube. The cooling jacket was then maintained at a constant temperature with a recirculating coolant.

The spot size, or field of view (FOV), of the thermopile detector was dependent on the geometry of its surroundings. The inner tube diameter of the cooling jacket was chosen to match the germanium window diameter of the thermopile detector. With reference to figure 12a, the diameter D of the FOV for an unconstrained detector can be determined from the geometry of the detector or by design the geometry of the cooling jacket:

$$\tan\alpha = \frac{(a-l)}{2y} = \frac{(D-l)}{2L} \tag{24}$$

The diameter D' of the region-of-interest (ROI), which is the constrained spot size, is calculated in a similar manner where

$$\tan\alpha' = \frac{(a-l)}{2y'} = \frac{(D'-l)}{2L} \tag{25}$$

The values for the variables in the two equations were obtained from either the manufacturer's specifications or the mechanical drawings and are listed in Table 2.

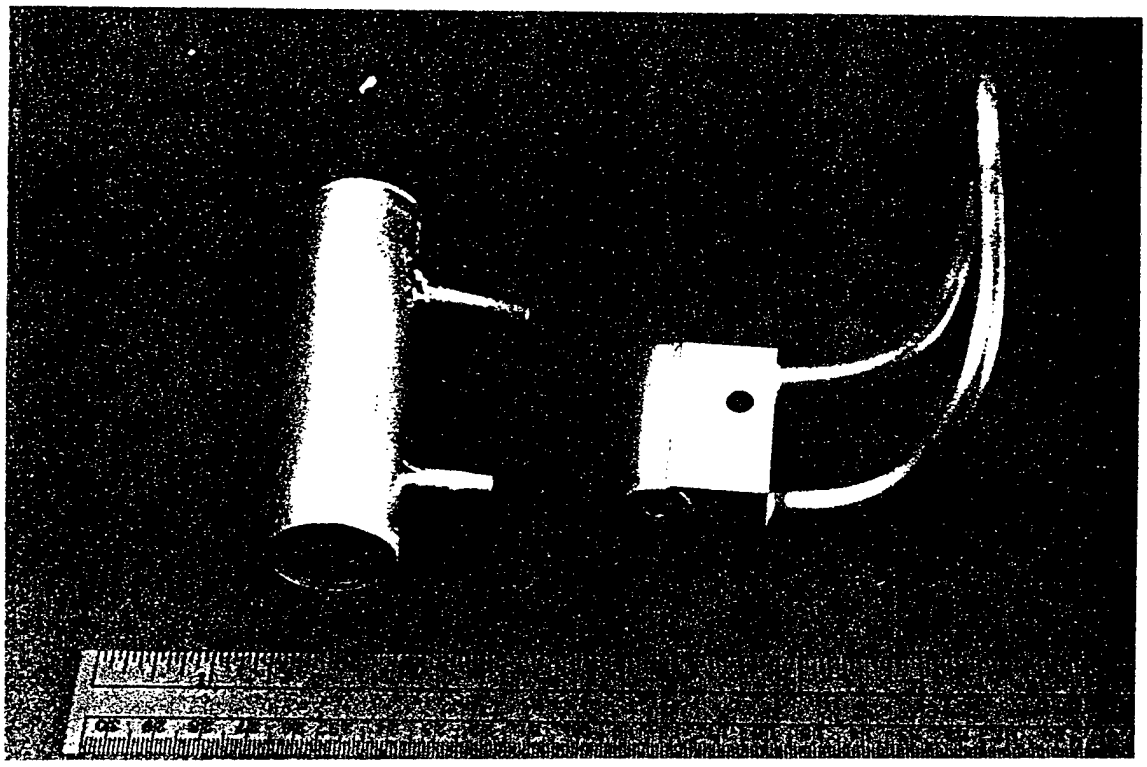

Figure 10. Photograph of copper cooling jacket used to maintain thermopile detector and signal head circuitry at a constant temperature. Large tube held instrumentation amplifier. Small tube was placed near welding arc and held thermopile detector.

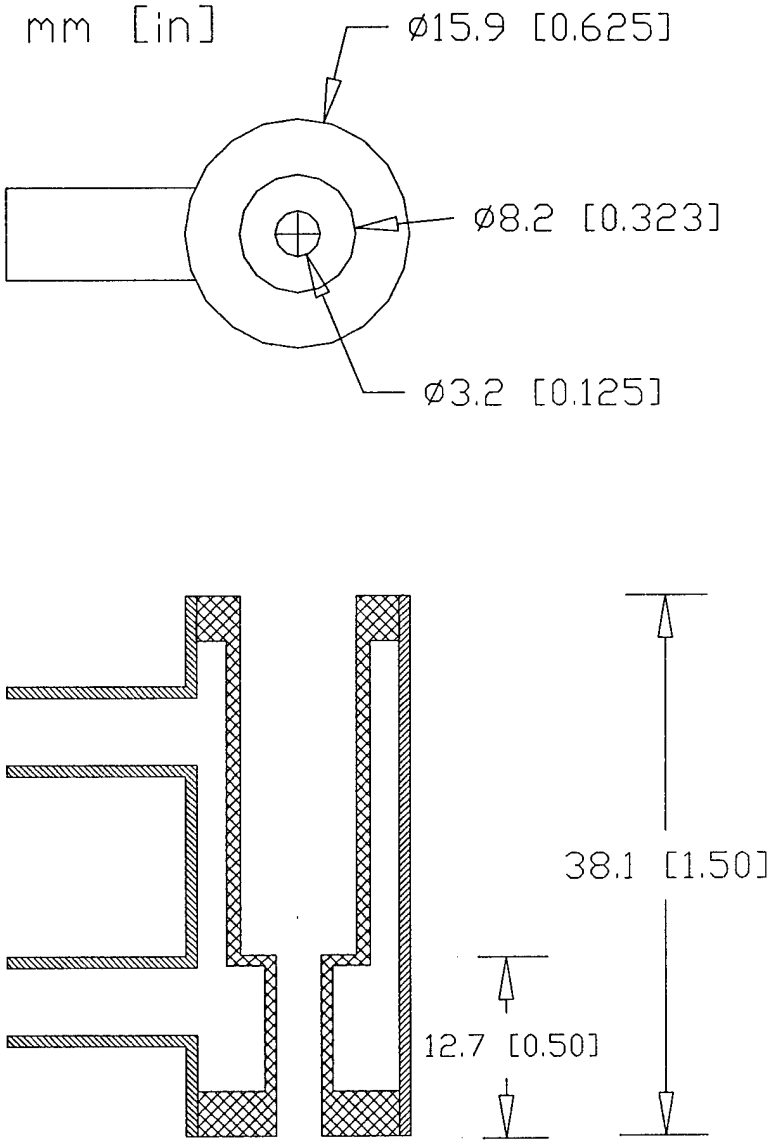

Figure 11. Mechanical drawing of small copper cooling jacket. Geometry of cooling jacket constrains the field of view of the sensor.

A plot of both of the spot size diameters, D and D', is shown in figure 13. The unconstrained spot diameter, D, increases rapidly as the distance to the target increases while the constrained spot diameter, D', slowly increases with the target distance. Since the detector was constrained by the cooling jacket, the FOV would be the projected area of the inner walls of the cooling jacket onto the surface of the target. A depiction of the ROI in the projected FOV is shown in figure 12b. The ROI occupies only a small portion of the projected FOV. The percentage of the ROI in the projected FOV is also shown in figure 13.

Table 2. Definition of Constants in Equations 24 and 25.

Variable	Description	Value
a	window diameter	3.94 mm
l	active film width	2.0 mm
y	distance to window	1.5 mm
y'	distance to end of tube	14.2 mm

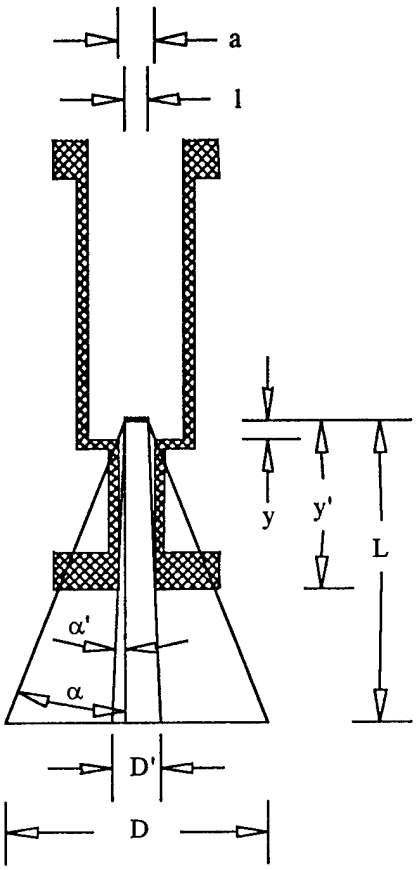

a. Geometry and notation used to determine sensor spot size

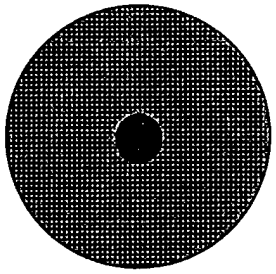

b. ROI (ϕ = D') in sensor FOV (ϕ = D)

Figure 12. a. Geometry of cooling jacket employed to calculate Region of Interest (ROI) and Field of View (FOV). b. Size and position of ROI to FOV.

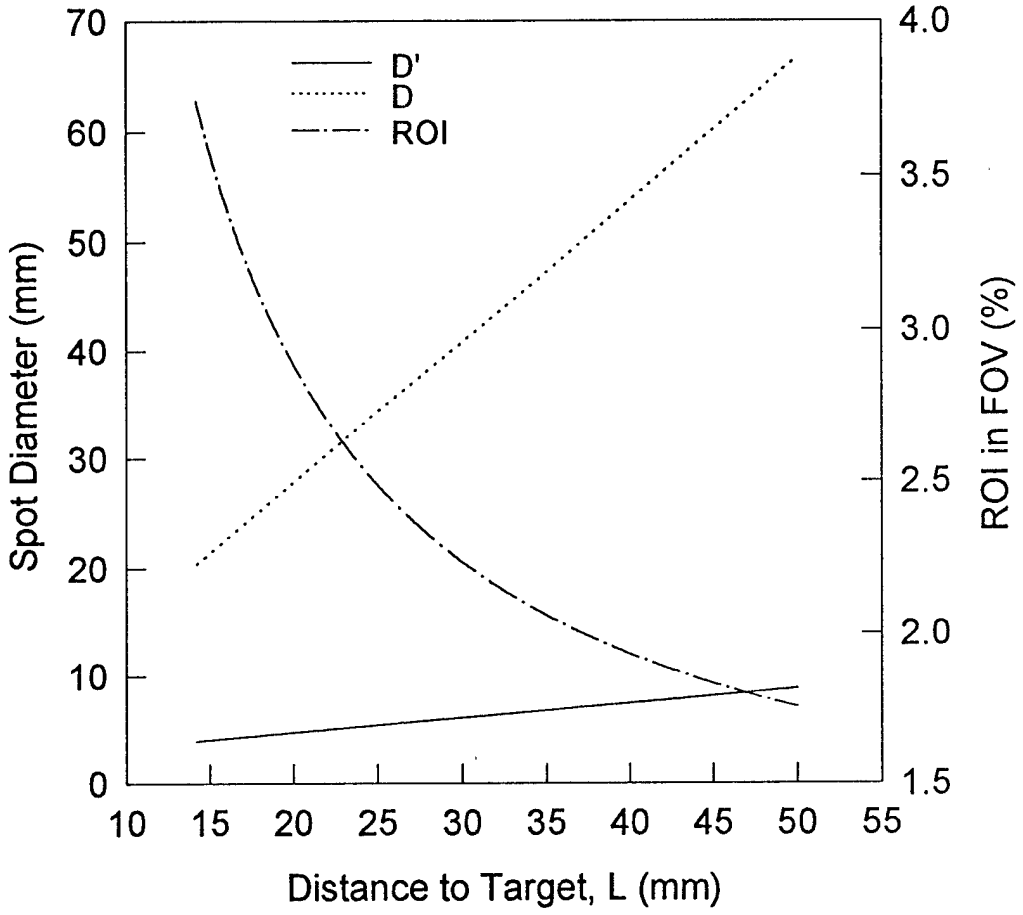

Figure 13. Spot diameter as a function of sensing element height. Constrained diameter, unconstrained diameter and the ratio between the two are shown.

Discussion

Modeling

The net heat exchange between the plate surface and the sensing element was calculated by combining a steady-state solution to the convection-diffusion equation with Equation 17. The net exchange was calculated for the cases of variable 1) radial position from the arc center, 2) angular displacement from the welding direction (polar angle), 3) and distance from the plate surface to the detector sensing element (target distance). The geometry and physical size of the cooling jacket were taken into account for these calculations. These calculations were performed for the welding conditions given in Table 3.

Table 3. Numerical model welding conditions

Parameter	Value
Current	120, 150, 180 Amps
Voltage	20 Volts
Welding Speed	2.54×10^{-3} m/sec

The effect of the polar angle on the net exchange is shown in figure 14 for a series of target distances and radial positions. Each figure corresponds to a different height, L, between the plate surface and the film sensing element of the thermopile detector. The distances, L, of 20.6, 26.9, 33.3, and 39.6 mm were used which corresponded to 6.35, 12.7, 19.05, and 25.4 mm (0.25, 0.50, 0.75, 1.0 in) between the plate surface and the bottom of the cooling jacket. For each figure (constant L), five radial displacements of the center of the sensor are plotted. These radial distances are 12.5, 17.5, 25.0, 37.5, 50.0 mm away from the center of the welding arc.

In each of the plots in figure 14, the largest exchange (top curve) corresponds with the closest radial distance, 12.5 mm, while the smallest exchange (bottom curve) corresponds with the farthest distance, 50 mm. As expected, the results of these calculations indicate that the greatest exchange of heat occurs behind the welding arc, for polar angles in the range $90° < \theta < 270°$. A polar plot of the same data as in figure 14a is shown in figure 15. This polar

representation of the data clearly shows the angular dependence of the heat exchange. The forward directions clearly show very little heat exchange with the sensing element.

A comparison between the net heat exchange and the sensing element height for a series of radial displacements is shown in figure 16. The net heat exchange decreases as the target distance increases. This is to be expected since Equation 6 has a $1/S^2$ dependence. A competing factor with this height dependence is the effect of height on the spot size or ROI of the sensor. The ROI increases as the sensor height increases. Close inspection of the net heat exchange versus height for the polar angle of 0°, figure 17, shows an increase in the exchange after an initial decrease as the sensing element height is increased for closest radial position of 12.5 mm. This increase is due to the fact that the ROI begins to encompass the steep temperature gradients on the plate surface where very high temperatures are encountered.

The relation between the target distance and the radial position can also be seen in figure 16. At a specific polar angle and a constant sensor height L, the radial position of the sensor has a large effect on the net heat exchange. As the sensor is moved away from the arc, the signal decreases rapidly. This is intuitive since there is a T^4 dependence on the net heat exchange and since most of the heat is concentrated near the arc. This indicates that the sensor should be as close as possible to the welding arc.

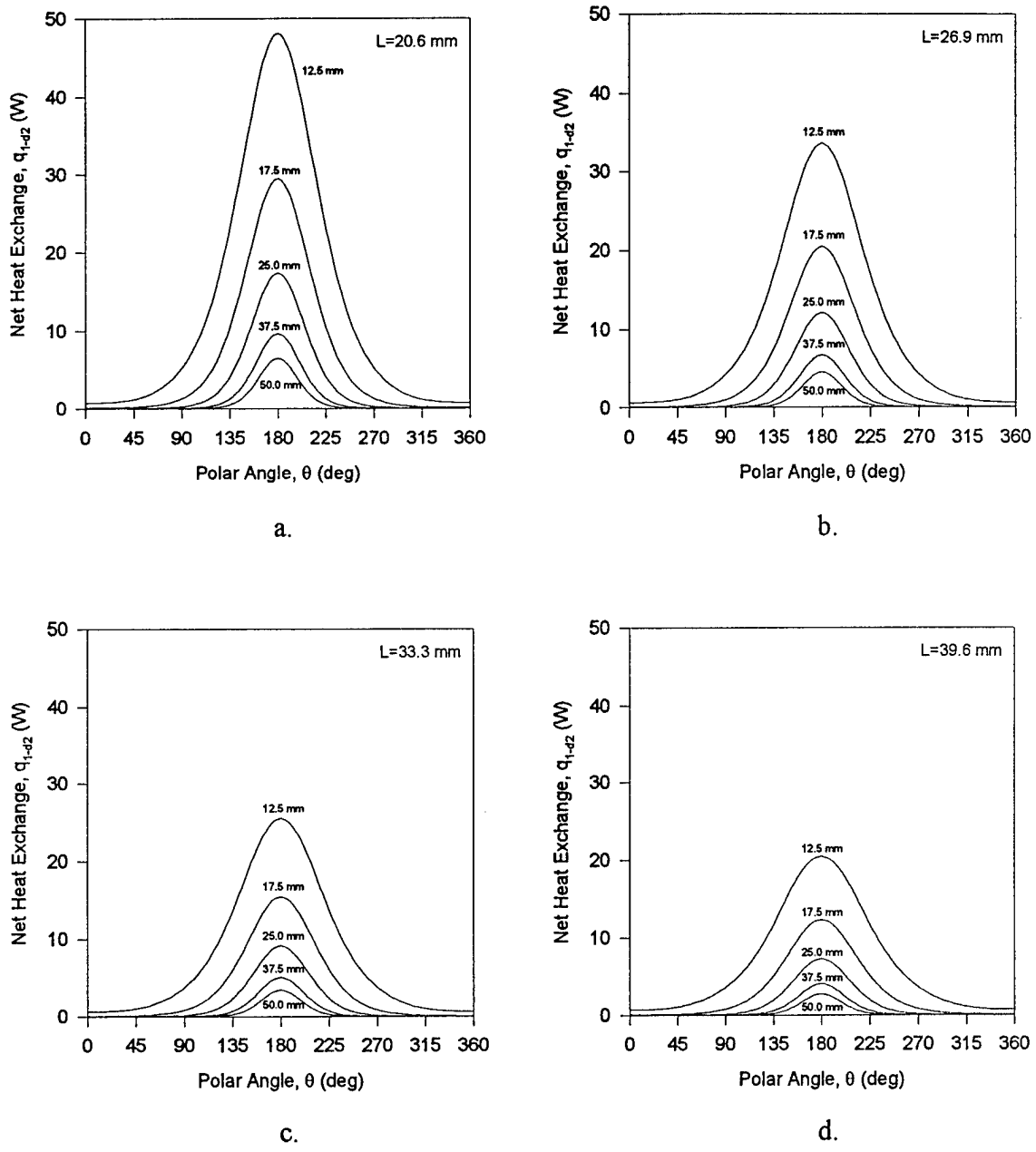

Figure 14. Calculated net heat exchange between plate surface and IR sensor. Each figure corresponds to a different height of the sensing element above the plate surface.

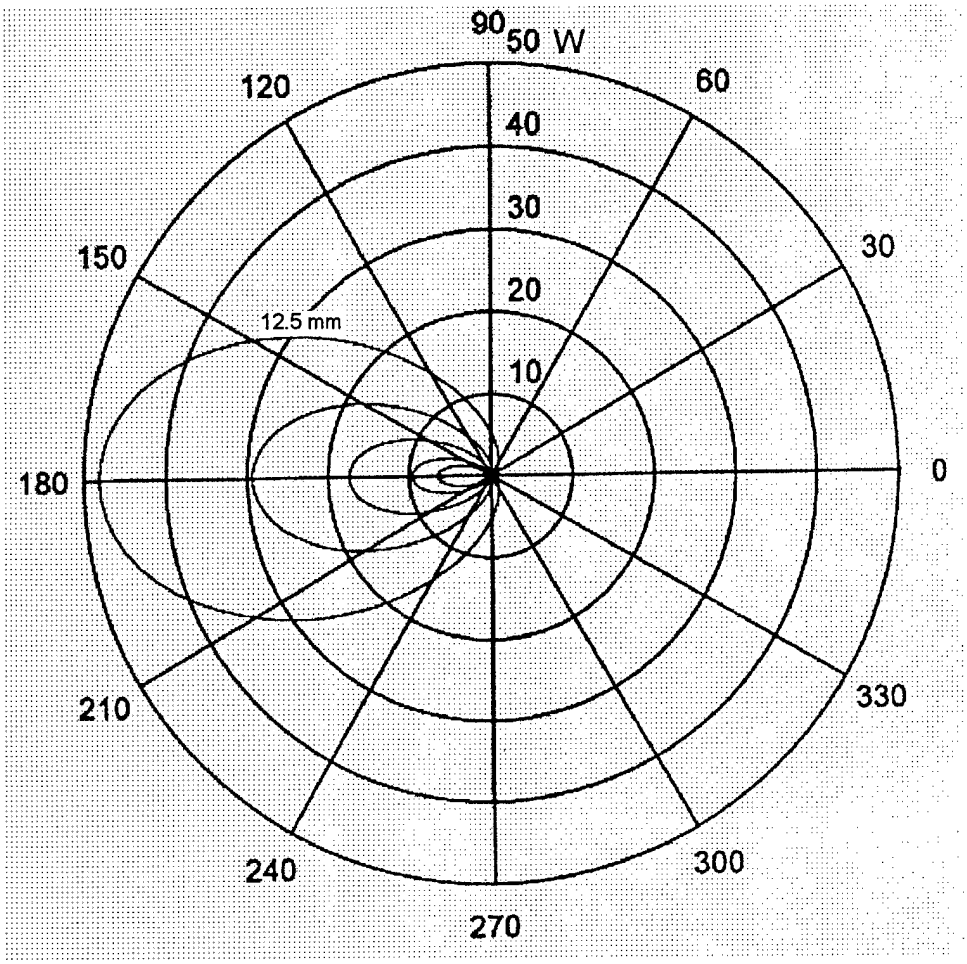

Figure 15. Polar plot of net heat exchange for a sensing height L = 20.6 mm. Greatest exchange occurs for the smallest radial distance.

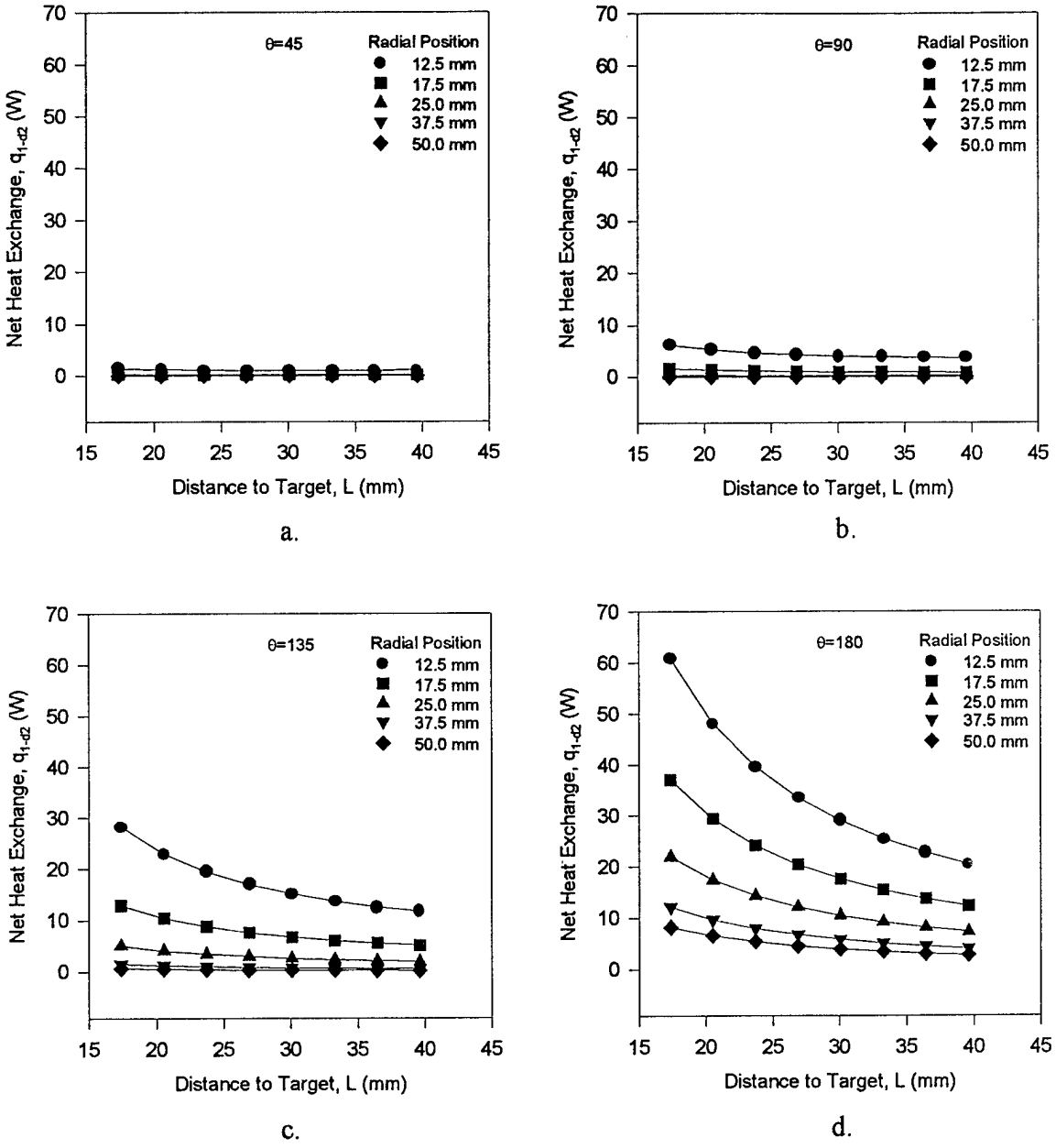

Figure 16. Effect of sensing element height on the net heat exchange for a series of polar angles for the IR sensor.

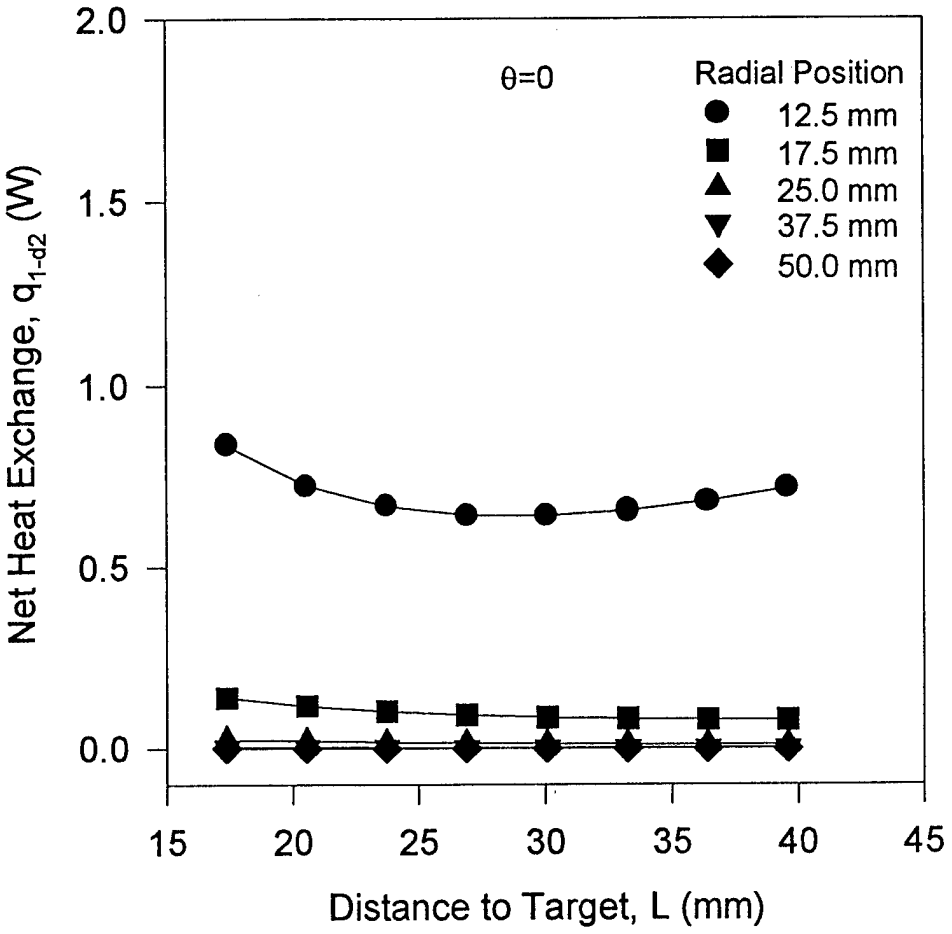

Figure 17. Magnified view of the net heat exchange for a polar angle $\theta = 0$.

The results of these calculations indicate that the greatest heat exchange between the plate surface and the thermopile detector occurs as close as possible to and behind the welding arc. Since the sensor signal is directly proportional to the net heat exchange, the greatest signal strength would also occur in this location. While this is the intuitive choice for the greatest sensor response, positioning the sensor in a rearward location is counterproductive for use in a welding process control system. As the sensor is positioned further behind the arc, the time lag between the phenomena that are occurring in the weld pool and the recognition of that phenomena increases. Figure 18 shows the time required to reach 95% of steady-state net heat exchange as a function of polar angle for different radial positions. The shortest times are in front of the arc center while the longest are directly behind the arc center.

Close inspection of all of the data show that at a polar angle of 90° for small radial displacements, the net heat exchange and thus the sensor signal begins to rapidly increase. This position is more acceptable for sensor placement during welding process control since it is directly perpendicular to the welding direction through the center of the welding arc. This eliminates any time lag due to positioning in the welding direction (x-direction with reference to the welding model) and leaves only the unavoidable lag due to displacement in the perpendicular direction (y-direction).

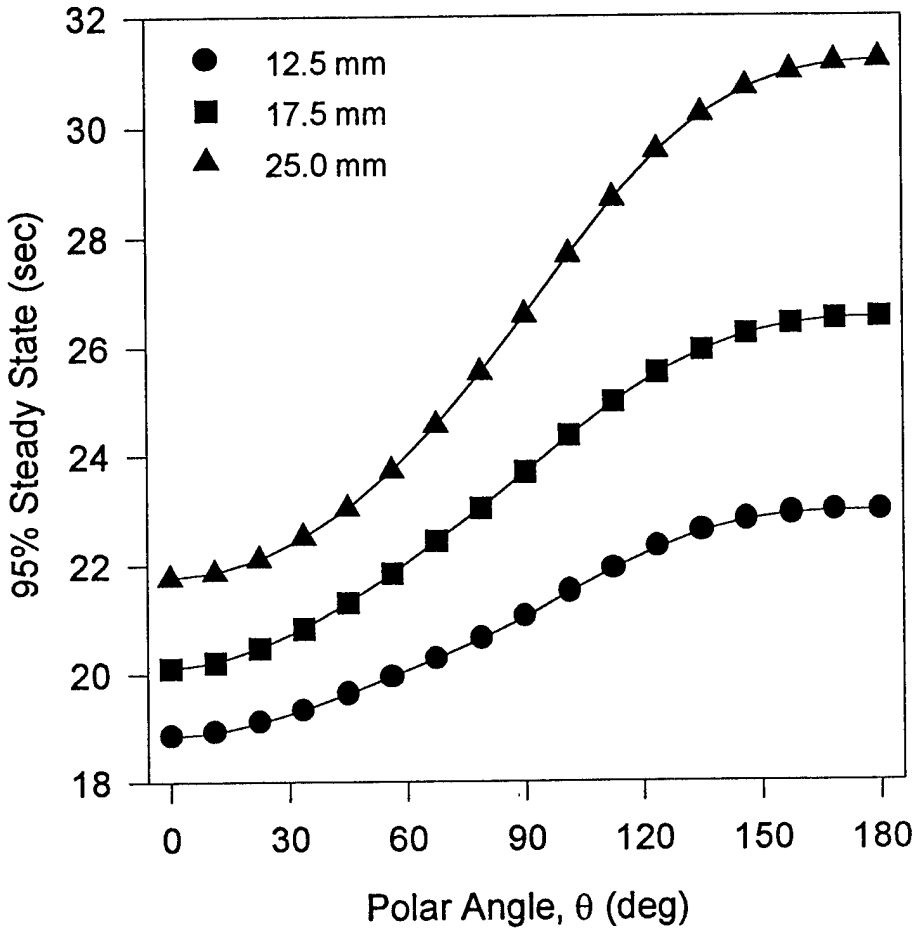

Figure 18. Time required for net heat exchange to reach 95% of its steady-state value after a step change in heat input of 2.4 to 3.6 kW as a function of polar angle.

Circuitry

The sensor's response to a step change in the target temperature was examined to determine whether the signal conditioning circuitry adversely slowed the response time of the system. The manufacturer's specifications listed a nominal time constant in the range of 150 to 350 msec. Measurements taken from oscilloscope traces such as that shown in figure 19 indicate that the time constant of the conditioned signal was approximately 300 msec, well within the manufacturer's nominal range.

A sinusoidal input was used to determine the frequency response of the signal conditioning unit. The effect of the filter on the sensor signal can be seen in the experimentally determined Bode diagram of the signal processor as shown in figure 20. At low input frequencies the signal passes through unchanged. However, as the input frequencies increase, the output signal is diminished. In this manner, high frequency signals such as ac line noise and welding arc noise are removed from the sensor signal. The measured phase lag between the input and the output signals appears to rapidly increase as the input frequency increases. This type of behavior is typical of the Butterworth filter though. This was not considered a major defect of the system since the process, which was being measured, changed very slowly and was thus essentially a dc-level signal and was not adversely affected by the filter.

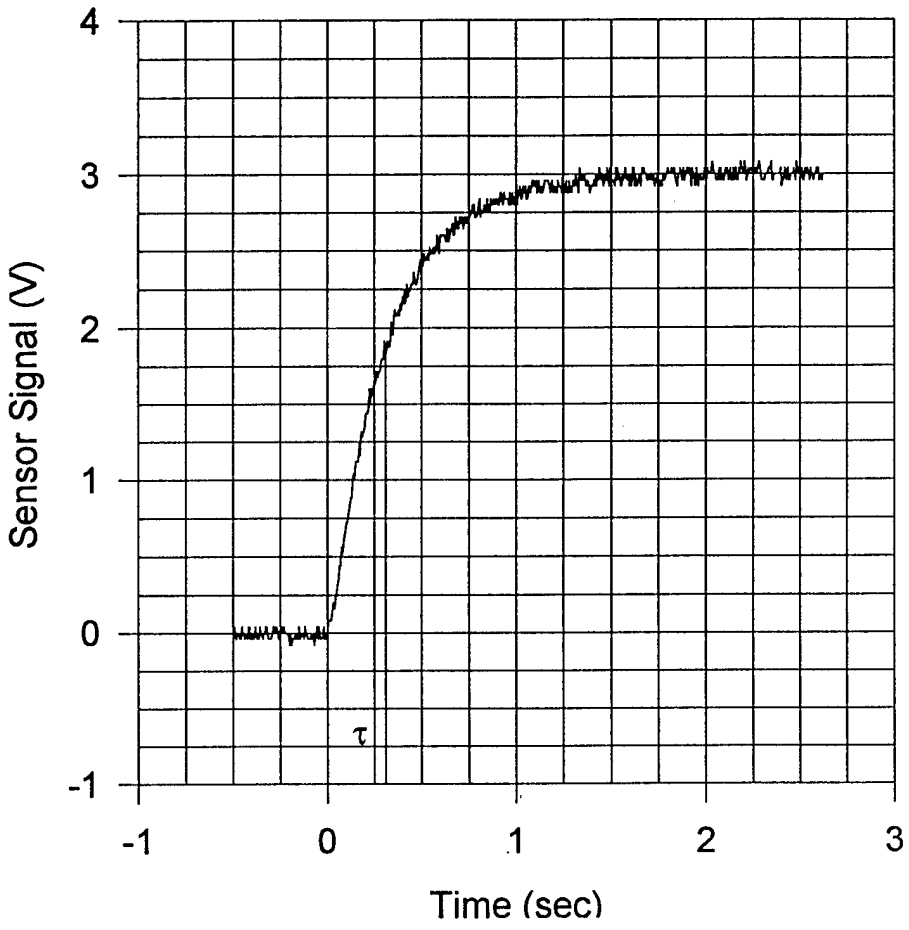

Figure 19. Oscilloscope trace of IR sensor signal after exposure to a sudden increase in its target's temperature.

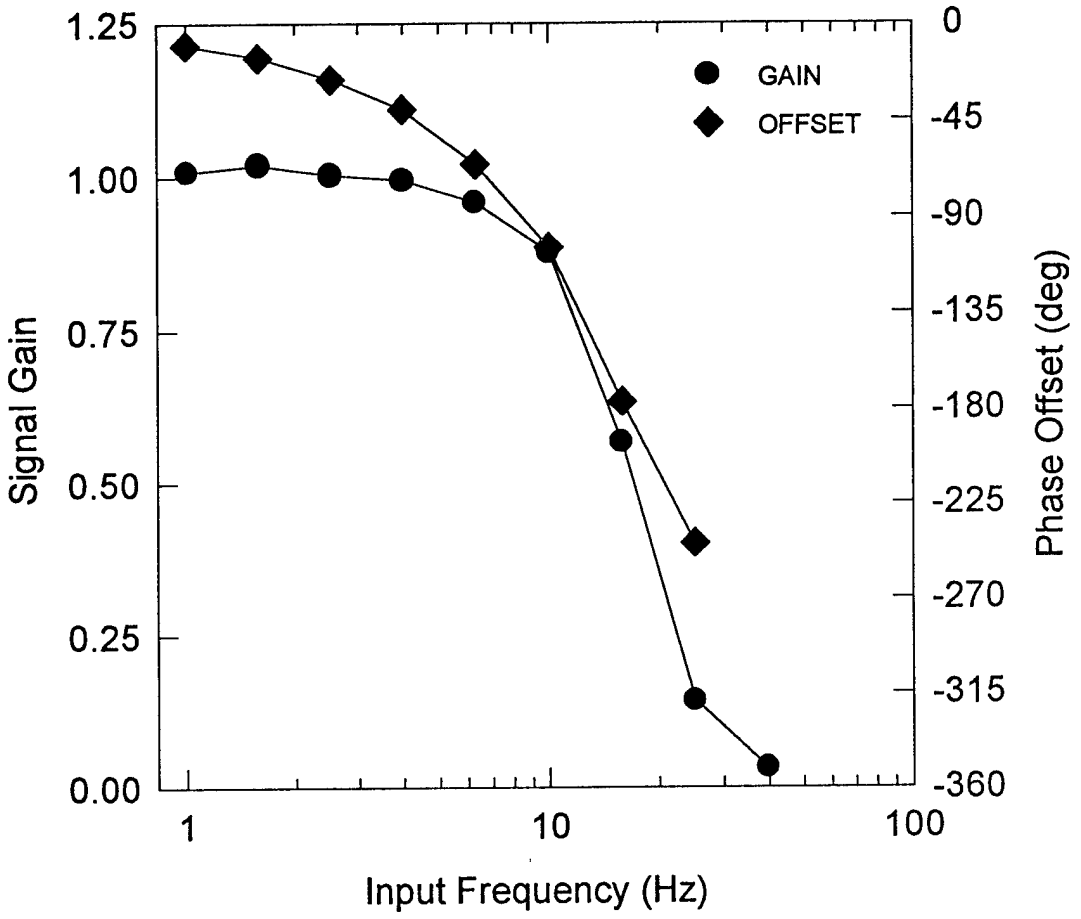

Figure 20. Measured performance of signal conditioning unit as a function of input signal frequency.

IV. CONTORL OF SUBMERGED ARC WELDING PROCESS

Using the developed infrared sensor, an integrated submerged arc welding feedback control system was built. This chapter will discuss the details of the design and development of the submerged arc welding control system and the feedback control results of specimens with different configurations using the developed system.

Experimental Details

Infrared Detector Housing and Cooling

As discussed above, the voltage generated by the thermopile detector is sensitive not only to the target temperature, but also to its own temperature. Hence, in order to maintain the detector at a constant temperature and shield it from the harsh welding environment, it was housed in a copper tube, which was cooled by a Vortex tube using compressed air. Since the detector is in physical contact with the copper tube, it is prevented from heating up and hence provides a signal which is representative of the target temperature.

The choice of vortex tube cooling was made after careful examination of actual shop floor welding conditions. Initially water-cooling had been proposed, but this would require a water source and recirculator or drain be located on the shop floor. While this could be accomplished, the use of water would have significantly increased the difficulty of adapting the proposed equipment to the shop floor. Hence, an alternative method of cooling using compressed air, which is available anywhere on the shop floor, was adopted. Air cooling also eliminated safety concerns related to waterlines breaking and coming into contact with welding power supplies, etc.

Torch Setup

The infrared sensor housed in a copper tube was attached to the submerged arc welding torch using an arrangement shown in the figure 21. The copper tube was attached to a stainless steel shaft capable of up-down motion with the help of linear bearings. The copper tube also has a wheel, which rests on the plate to be welded. This ensured a constant sensor to the plate surface distance to be maintained even in the case of distorted plates and allowed the sensor to travel along the weld. This torch attachment also allows easy adjustment of the position of the

sensor with respect to the welding electrode. The sensor views the plate surface close to the weld and the excess flux in the view of the sensor was removed using a vacuum extractor. The sensor was placed 20 mm from the wire electrode in a direction perpendicular to the travel direction and about 40 mm above the surface of the plate.

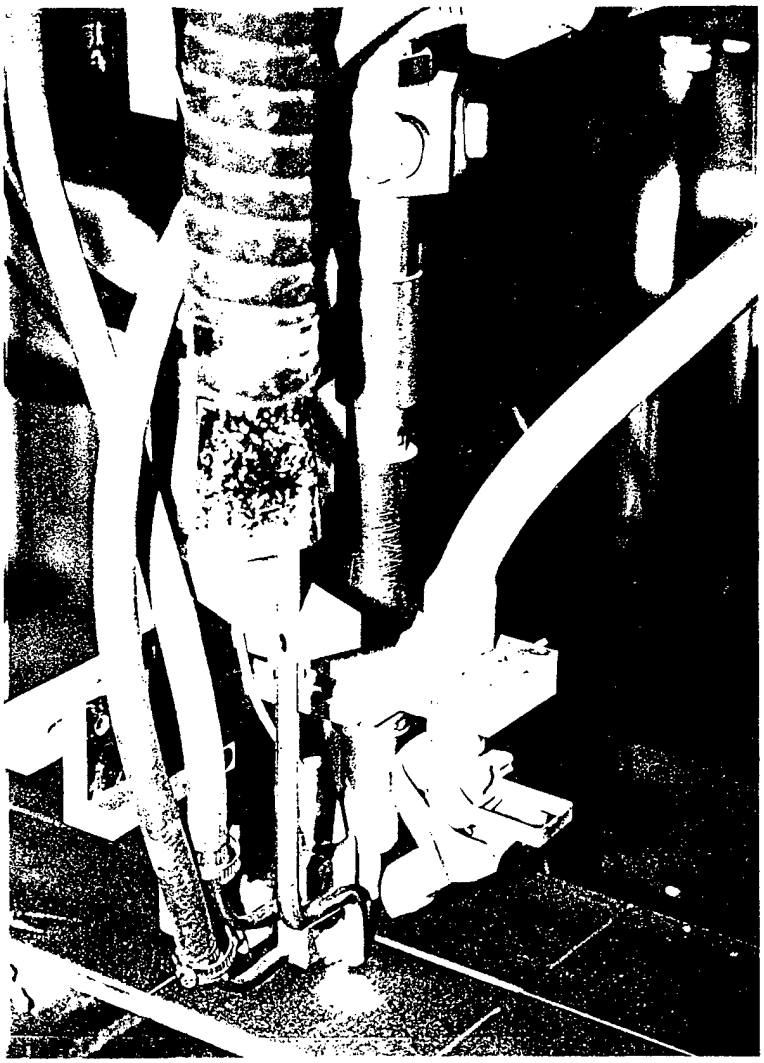

Figure 21. Photograph showing the torch attachment.

Data Acquisition System

The data acquisition system consisted of the DaqPad 1200 data acquisition card, terminal board and signal isolator/conditioning modules. The data acquisition card is capable of 12 bit (1 in 4096) resolution for both the analog-to digital (A/D) and digital-to-analog (D/A) conversions. The data acquisition unit has eight input channels and two output channels and was configured for the 0 to +10 volts range. Signal gain was set at 1 for all experiments. The resolution of the voltage scale is given by

$$resolution(V) = \frac{range(V)}{gain \times 2^{resolution}} \tag{26}$$

With the above mentioned settings, the signal resolution was 2.44 mV for both the input and output channels. The acquisition card is capable of acquisition rates up to 100 K/s with a conversion time of 8.5 μs. All the external signals were electrically isolated using optical isolators in order to separate the electrical grounds and to prevent damage to the card and the computer. The conditioned IR signal and the arc voltage were acquired at an average rate of 120 readings per second. The arc voltage was reduced to 0 to +10 volt range using a voltage divider circuit before being acquired.

SAW Machine Electronics Modification

Since the submerged arc welding power supply is of constant voltage type, the welding current is controlled by changing the wire feed speed. The machine electronics were modified to facilitate direct control of the wire feed speed (welding current) and the arc voltage from the computer. The wire feed speed and arc voltage potentiometers on the control panel were bypassed using double pole/double throw switches and the control signal from the computer was directly passed on to the machine electronics.

Welding Process Controller

The welding control system program was written in a graphical language 'G' using the software package LabVIEW from National Instruments. A Virtual Instrument Weld Machine

Controller which facilitates the control of the welding variables from the computer screen was created as shown in the figure 22. The software routines were built using Virtual Instruments (VI), a graphical representation of a subroutine or function. Each VI was composed of two parts namely, a front panel and a diagram. The front panel serves as the user-friendly interface between the computer and the user, and handles all the input and output. The diagram shows the program code, which was developed by wiring together the subVI's. The LabVIEW program differs from the traditional text based program by the manner in which the instructions are executed. Text based programs execute in a top-down fashion, beginning with the first statement and executing one statement at a time. In contrast, LabVIEW, which is a data flow language, executes the instructions when all of the necessary data is available at its inputs. Thus many subVI's are executed simultaneously, making the position of the subVI on the diagram irrelevant. The data is passed between the subVI's through wires, which may be of different designs and colors depending on the data type.

The program consists of analog input, process controller for welding current and arc voltage, file input/output and analog output paths. Each path consists of configuration, initialization, action, error checking and termination (stop). The action and error checking steps occur inside a while loop that iterates at a specified rate until the stop button on the front panel is depressed or an error occurs. The data acquisition begins at the start of the programs and each channel is sampled at a high rate to avoid aliasing effects. The acquired data is smoothed using averaging methods, and the smoothed data is then used for the process control. A proportional/integral/derivative (PID) control technique was used for the control of the welding current and the arc voltage. In the discrete form, the control algorithm, which is a differential equation, was solved for each iteration of the control loop. The IR sensor signal and arc voltage were the measured variables, whereas the wire feed speed and the arc voltage were the manipulated variables. The PID control parameters were determined using the Zeigler-Nichols tuning procedure and by performing weld trials.

The IR sensor signal, arc voltage, the process set points and control outputs are displayed on the front panel screen of the VI weld process controller. The data is also stored in an ASCII format for further analysis and presentation. Initiating the automatic control caused the IR

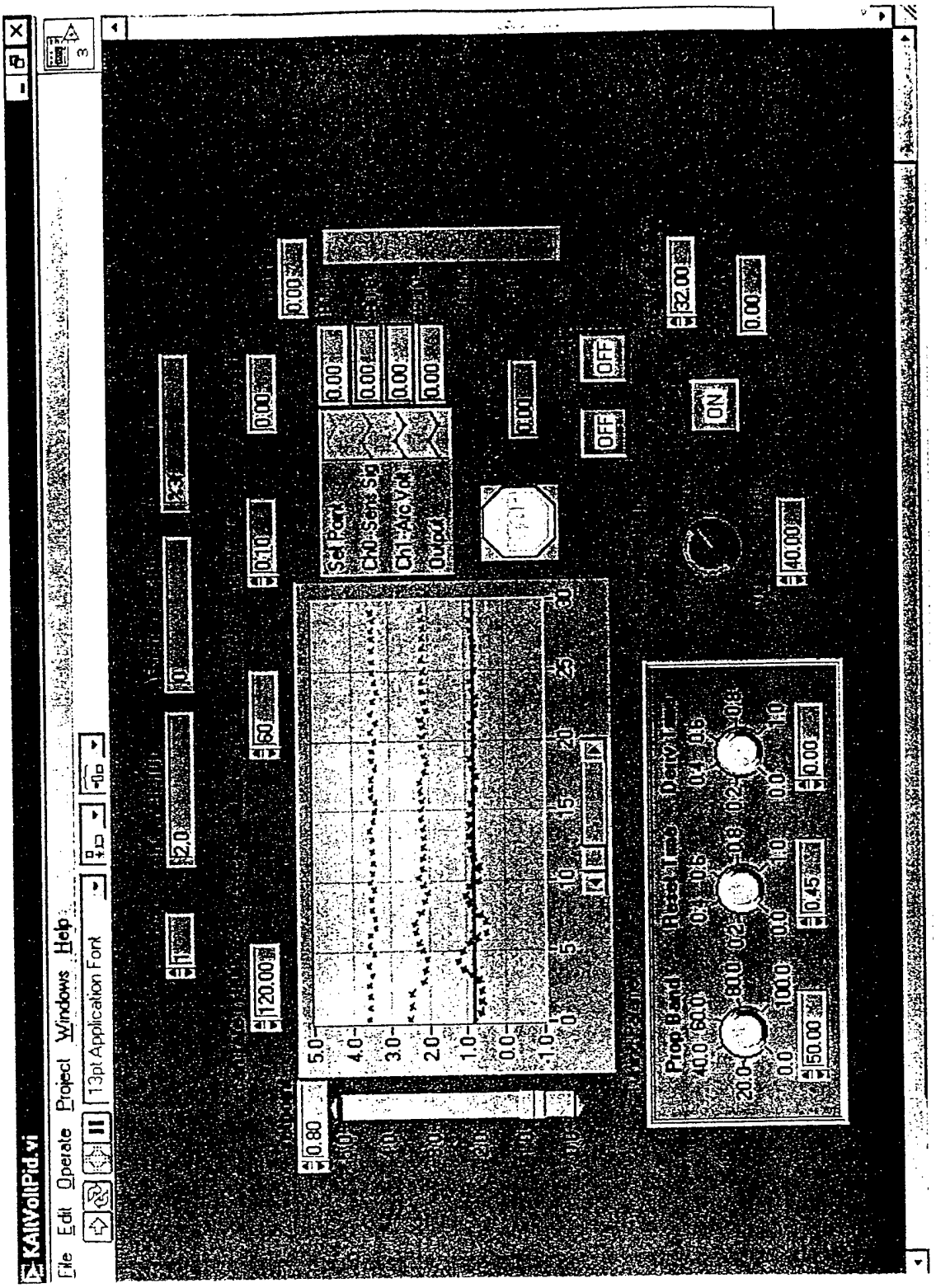

Figure 22. Virtual Instrument Weld Process Controller.

sensor signal and the arc voltage to be maintained at respective set points through the control of the wire feed speed and arc voltage. The control system takes corrective action when perturbations upset the process, i.e., after the temperature of the plate has changed from the set point.

Welding Equipment and Consumables

All the submerged arc welds were made using a L-TEC VCR-801 constant voltage, direct current power supply capable of providing 800 amperes of current. The movable welding head was mounted on a horizontal beam. The instrument panel on the welding head contained the controls for travel speed, wire feed speed and the arc voltage. L-12 carbon steel electrode wire of 1/8 inch in diameter and of composition 0.07-0.15% Carbon, 0.35-0.6% Manganese and 0.05% Silicon, and Lincoln WeldFlux 780 conforming to AWS A5.7-69 were used to produce the welds. Hot rolled AISI 1008 carbon steel plates were used in all experiments. The plates were sandblasted or ground to remove rust and mill scale on the surface.

Results and Discussions

IR Sensor Signal, Welding Current and Control Signal Relationships

Bead-on-plate welds were performed at different welding current values, keeping other parameters constant to analyze the relationship between the IR sensor signal, welding current and the controller signal. The welds were performed on 1/4 inch thick hot rolled plates with sandblasted surface. The IR sensor signal was obtained by averaging the values in the stable region of the weld. A linear relationship was found to exist between the IR sensor signal and the welding current as shown in the figure 23. A linear relationship was also found to exist between the control signal and the welding current as shown in figure 24.

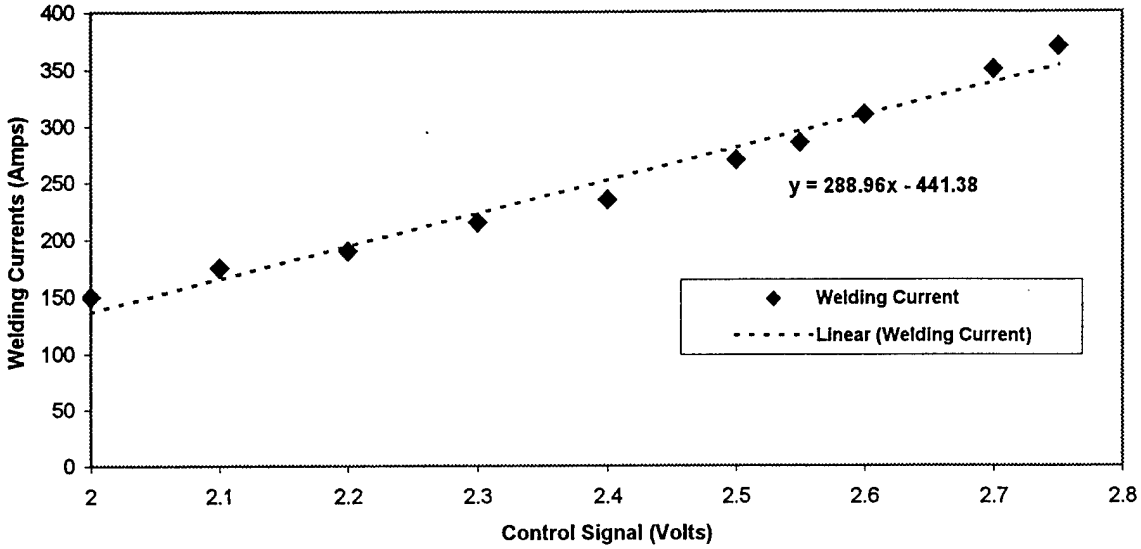

Figure 23. Infrared Sensor Signal Vs Welding Current

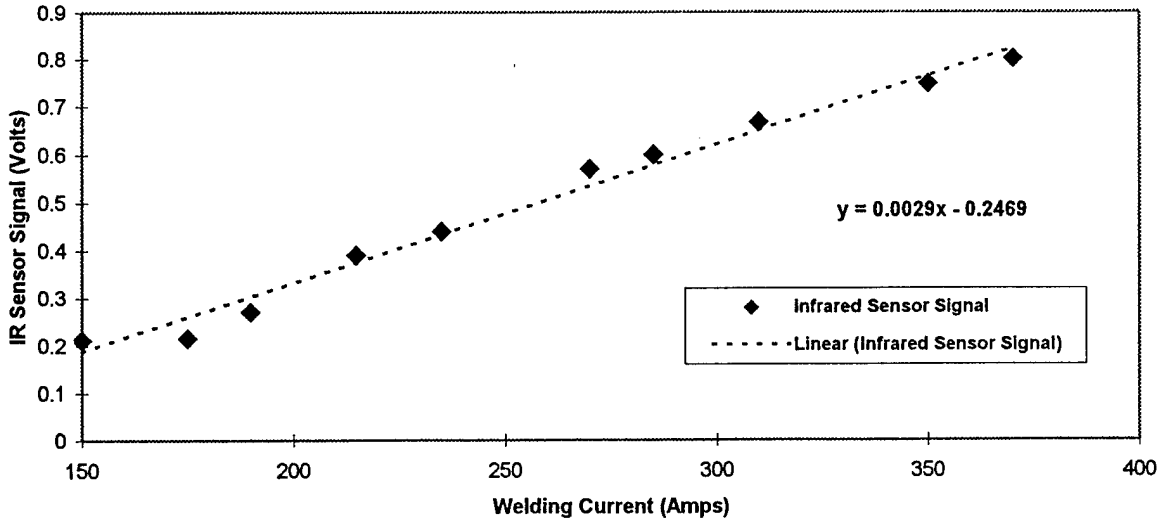

Figure 24. Welding Current Vs Control Signal

Constant Thickness Plate Welding Trials

Bead-on-plate welding trials were performed to acquire the IR sensor signal for plates with constant thickness. The plates were of dimensions 24" X 6" X 3/8". The welding conditions used for the trials were,

Welding Current	:	370-400 amps
Arc Voltage	:	26-28 volts
Welding Speed	:	9 inches/minute

For welds performed with constant welding current, the IR sensor signal increased and then reached a constant value as the weld progressed as shown in figure 25. Since there were no disturbances introduced, the IR sensor signal remained constant till the end of the run. In the case of welds performed using the IR sensor feedback control, the IR sensor signal was controlled at the set point by the weld process controller as shown in the figure 26. The error between the set point and the IR sensor signal was used by the controller to adjust the wire feed speed (welding current). The control was started after the welding process (IR sensor signal) reached an initial steady state condition.

Step Thickness Change Plate Welding Trials

Bead-on-plate welding trials were performed on plates with step change in thickness to investigate the performance of the weld process controller. The step change in the plate thickness was used to induce disturbance in the thermal distribution around the weld pool. The welds were performed on plates with dimensions 24" X 6" X 3/8". The thickness was reduced to 1/4" at the region of the stepped thickness change for 6" long at the center of the plate. Figure 27 shows the schematic of the stepped plate used for the welding trials. The welding conditions used were,

Welding Current	:	370-400 amps
Arc Voltage	:	26-28 volts
Welding Speed	:	9 inches/minute

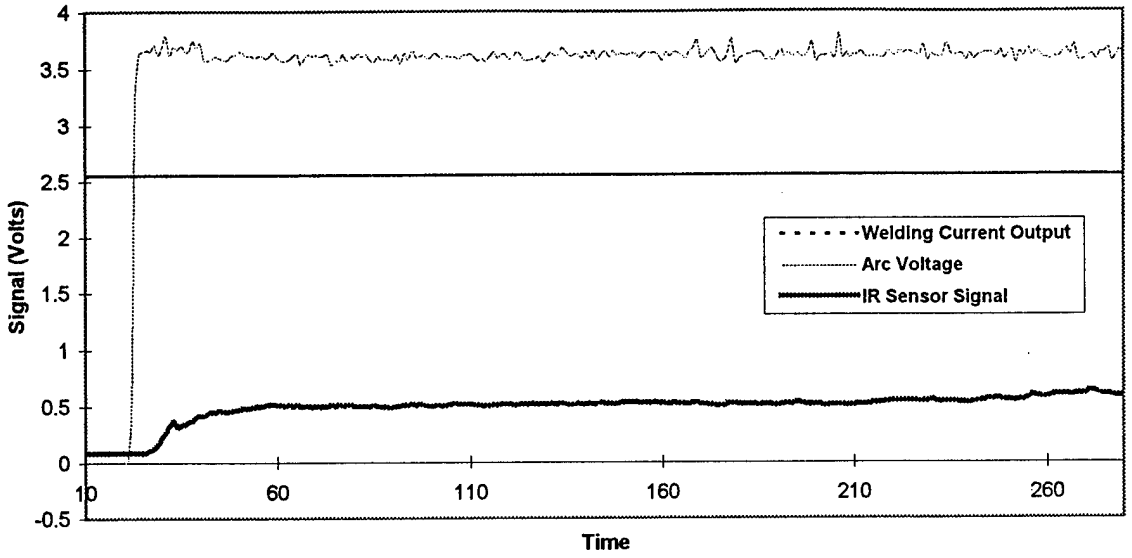

Figure 25. Graph showing the IR sensor signal, arc voltage and welding current output for weld performed with no control on constant thickness plate.

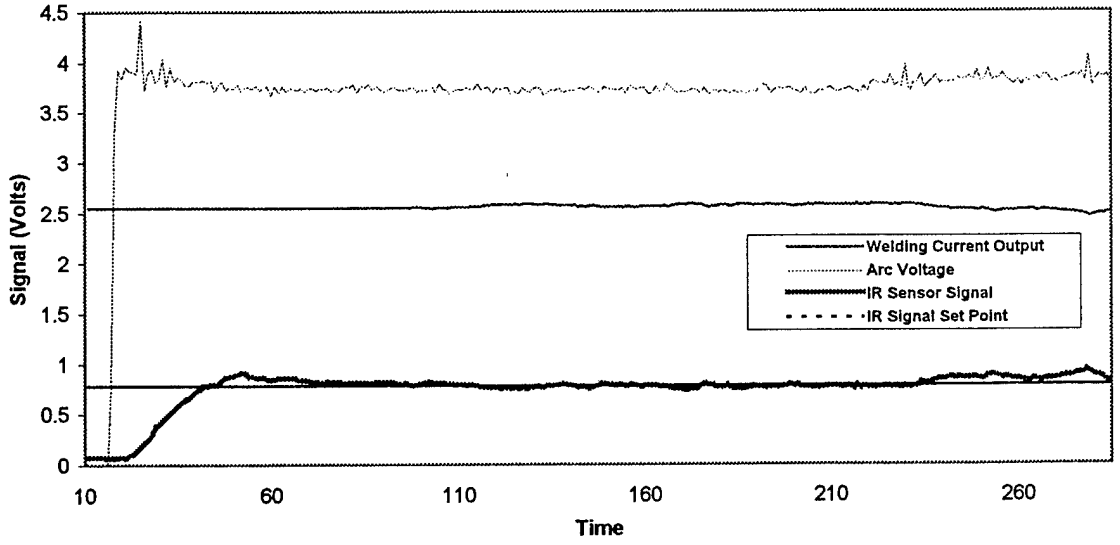

Figure 26. Graph showing the IR sensor signal, arc voltage, welding current output, and IR signal set point for weld performed with automatic control on constant thickness plate.

Welds performed with constant current (no control) showed an increase in the IR sensor signal at the region of the step change in the thickness. The IR sensor signal increased due to the increase in the heat input/unit mass at the region of the step as shown in figure 28. When automatic control was used, the controller sensed the increase in the IR sensor signal and correspondingly decreased the wire feed speed thereby preventing burn through at the region of the reduced thickness - figure 29. Welds performed with the same welding current but without control caused burn through to occur. Figure 30 shows the picture of the top and bottom sides of the plates welded with and without control.

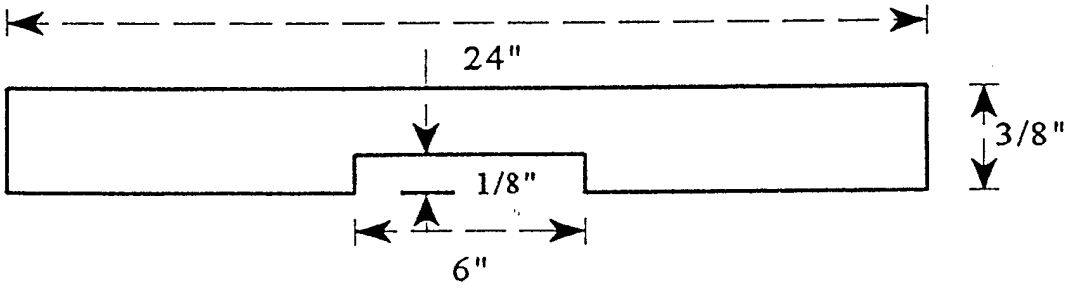

Figure 27. Schematic of the stepped thickness plate.

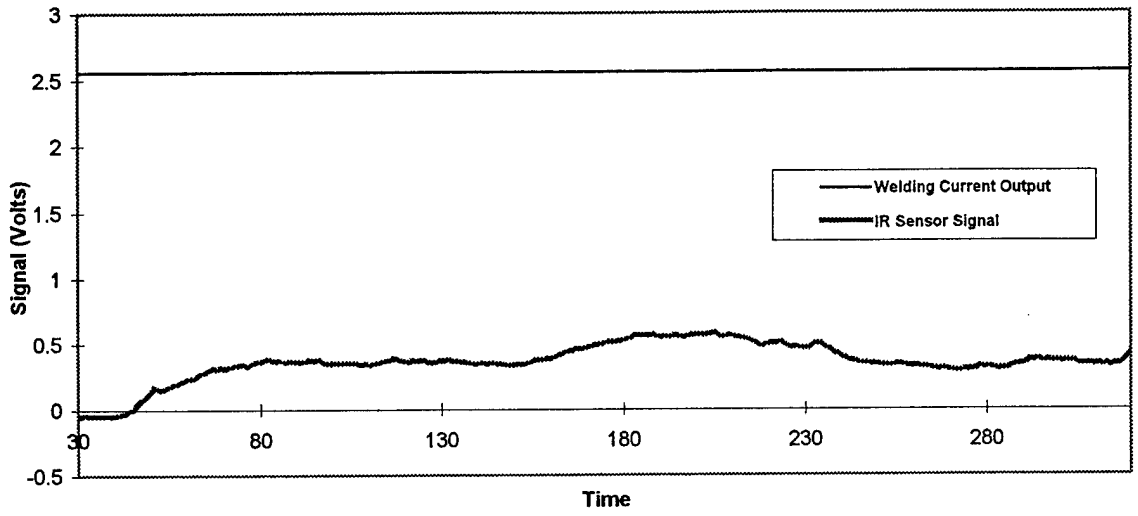

Figure 28. Graph showing the IR sensor signal and welding current output for the weld performed with no control on a plate with stepped change in thickness.

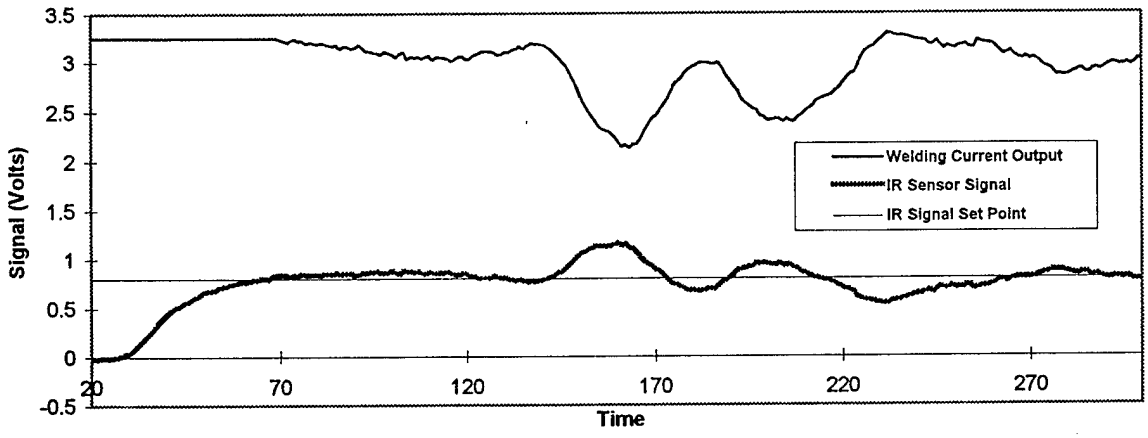

Figure 29. Graph showing the IR sensor signal, welding current output and the IR signal set point for a weld performed with automatic control on a plate with step change in thickness.

No Control

With Control

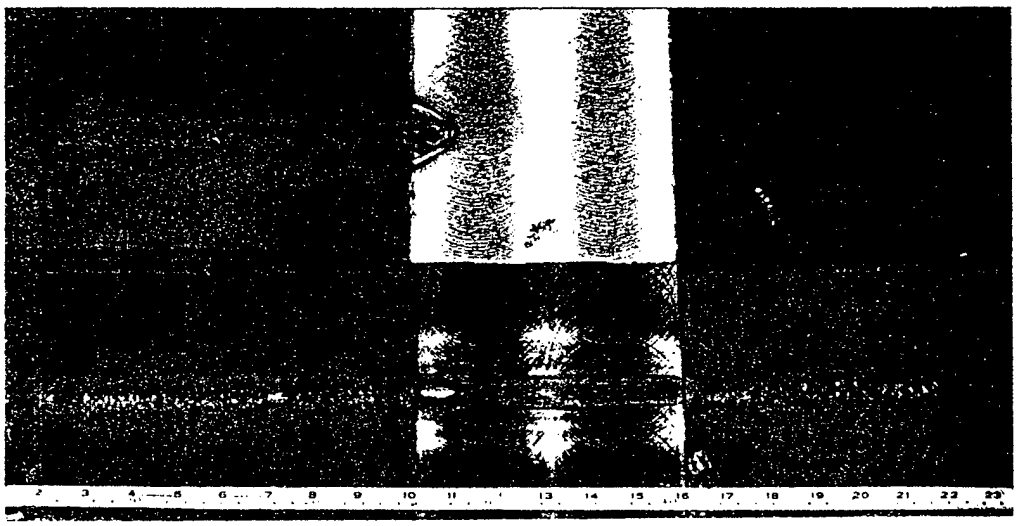

No Control

With Control

Figure 30. Photograph of the top and bottom sides of plate with step change in thickness welded with and without automatic control.

Butt Joint Welding Trials

Butt joint welding trials simulating the shop floor conditions in the shipyard were performed using plates of dimensions 24" X 4" X 3/8" to study the performance of the weld process controller. Initially, partial penetration welds were performed with and without automatic control on both sides of the square butt joints with constant gap, to achieve constant penetration and proper filling of joint gaps. The joints were radiographed to check for slag inclusions, improper side wall fusion and incomplete penetration. The joints tested did not contain these defects and passed the radiography test. These trials helped in fixing the proper welding conditions for the butt joint trials. The welding conditions used were,

Welding Current	:	350-450 amps
Arc Voltage	:	26-28 volts
Welding Speed	:	9 inches/minute

Trials on Butt Joints formed with Plates of Equal Thickness

Extensive butt joint welding trials were performed using plates of dimensions 24" X 4" X 3/8". Butt joint trials were also performed using plates of dimensions 36" X 4" X 1/4" and 36" X 4" X 1/2". Butt joints with constant gap and sudden variable gap were performed to investigate the performance of the weld process controller.

	Butt Joint Combination		
Constant Gap	1/4-1/4	3/8-3/8	1/2-1/2
Variable Gap	1/4-1/4	3/8-3/8	1/2-1/2
Welding Current	320 amps	410 amps	485 amps

Figure 31 shows the schematic of the joint design used for the welding trials. In the case of joints with variable gap in which the gap was increased from 1/16" to 1/8" for 5" long, the IR sensor signal increased corresponding to the region of wider gap due to the higher heat input/unit mass as shown in figure 32. In the case of welds performed using automatic IR sensor feedback control, the controller sensed the increase in the IR sensor signal corresponding to the region of

the increased gap and decreased the wire feed speed (welding current) thereby preventing burn through as shown in figure 33. Welds performed without control but at the same initial welding current caused the weld pool to collapse leading to burn through at the region of increased gap. Figure 34 shows the picture of the butt joint weld with variable gap performed with automatic control.

Trials on Butt Joints formed with Plates of Different Thickness

Butt joint welding trials were performed using plates of different thickness in order to simulate the welding of ship hull plates. Butt joints are made using plates of different thickness combinations, as shown in the table below. Both constant gap and variable gap butt joint trials were performed in order to investigate the performance of the weld process control.

	Butt Joint Combination		
Constant Gap	1/4-5/16	5/16-7/16	7/16-1/2
Variable Gap	1/4-5/16	5/16-7/16	7/16-1/2
Welding Current	360 amps	430 amps	470 amps

The variable gap was formed in the plate of smaller thickness in the case of all combinations for the welding trials. The variable gap was 8" long and about 1/8" wide. The IR sensor showed an increase corresponding to the increased gap and the controller decreased the welding current thereby preventing burn through. These experiments indicate that the IR sensor weld controller system can be used in case of butt joints formed using plates with different thickness.

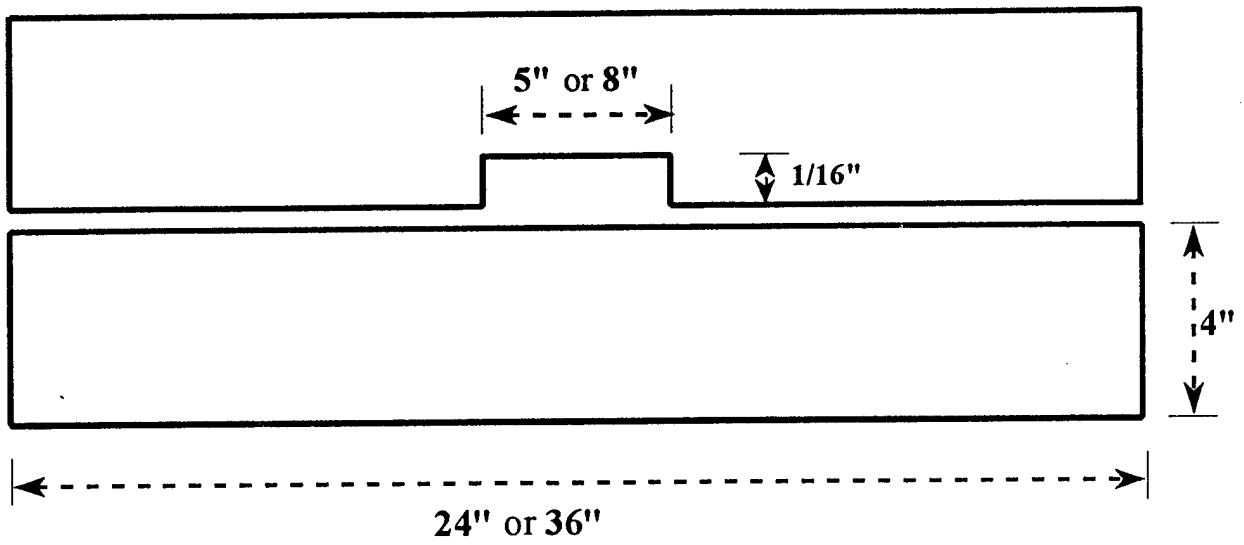

Figure 31. Schematic of the butt joint design with variable gap used for welding trials.

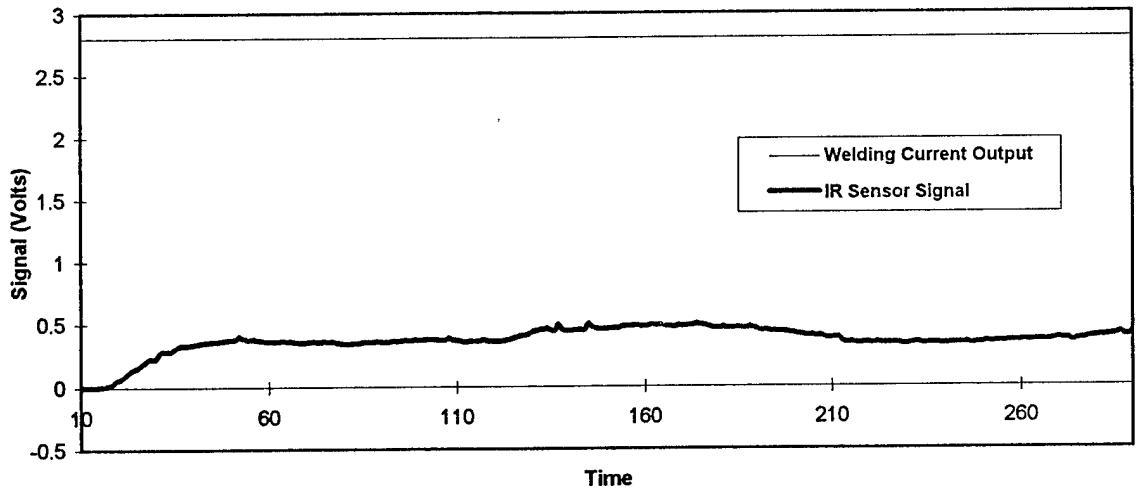

Figure 32. Graph showing the IR sensor signal and the welding current output for butt joint with variable gap performed without automatic control.

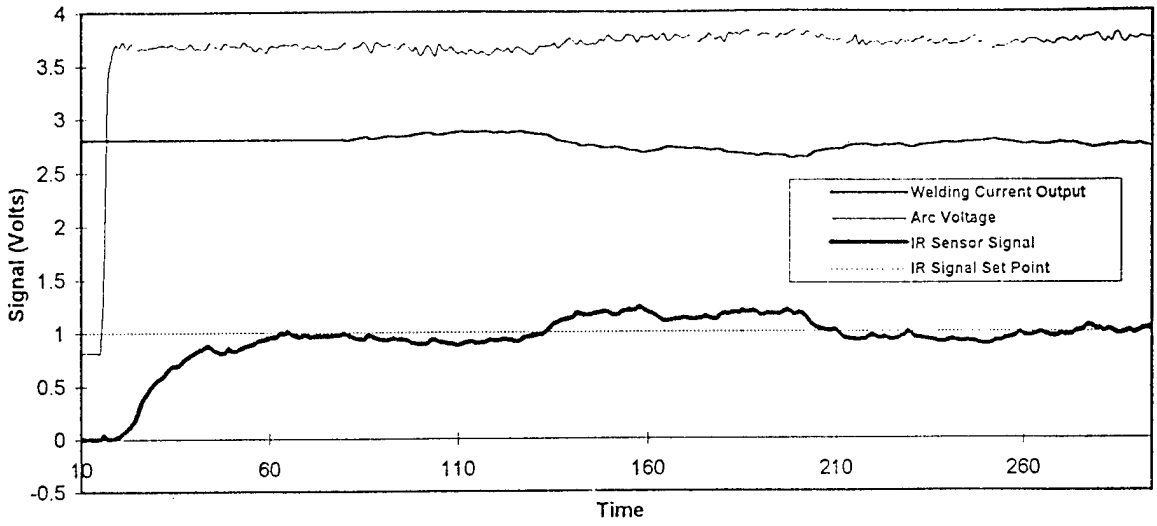

Figure 33. Graph showing the IR sensor signal, arc voltage, welding current output and the IR signal set point for butt joint with variable gap performed with automatic control.

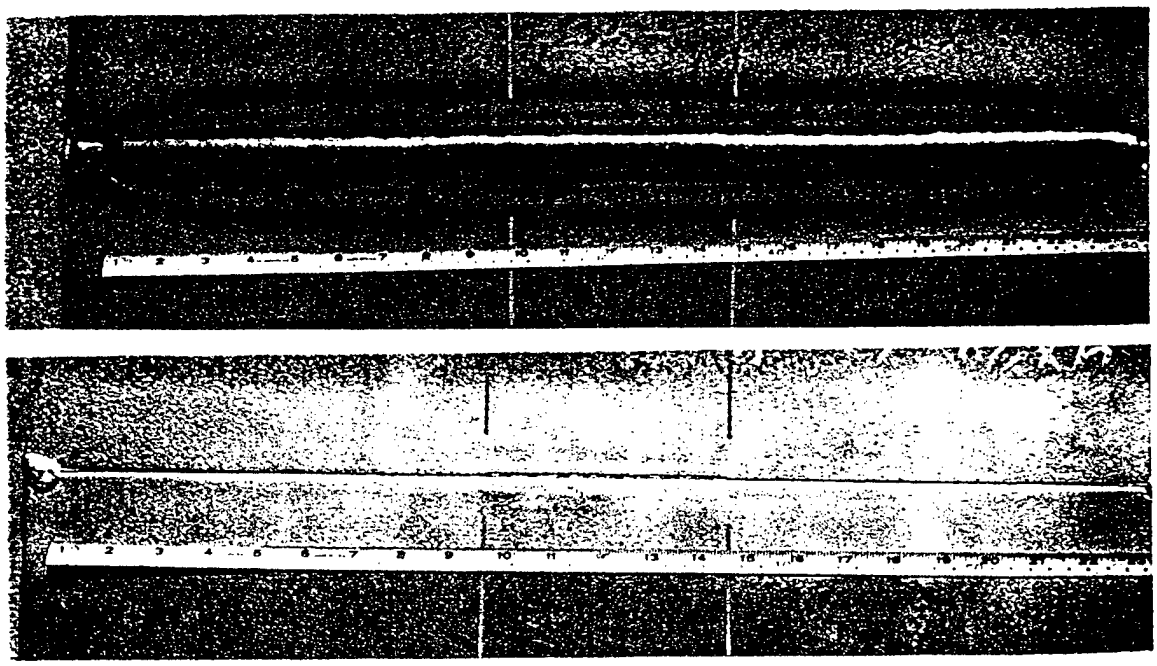

Figure 34. Photograph showing the top and bottom sides of butt joint weld with variable gap performed with automatic control.

Arc Voltage Control

Since arc voltage is also a parameter in controlling the heat input, it is important to control not only the welding current but also the arc voltage. The arc voltage also affects the bead shape and hence the thermal distribution in the plate. Hence it is pertinent to control the arc voltage also to achieve proper penetration control. Although constant voltage power supplies have been developed to provide constant voltage even when the welding current is changed, true constant voltage is never achieved. The extent of the variation of the arc voltage depends on the design of the power supply, i.e., its Volt-Ampere characteristics as shown in the figure 35. To achieve constant voltage in scenarios where the welding current changes, it is required to change the arc voltage setting in real-time. Bead-on-plate welding trials in which the arc voltage was changed while other parameters were kept constant showed a corresponding change in the IR sensor signal as shown in the figure 36. Figure 37 shows the change in the arc voltage when the welding current is decreased. Therefore to achieve proper control, arc voltage control was implemented in addition to the control of the welding current. In the case of welds made with automatic control of the welding current and the arc voltage, even when the current decreased, the arc voltage remained constant as shown in figure 38.

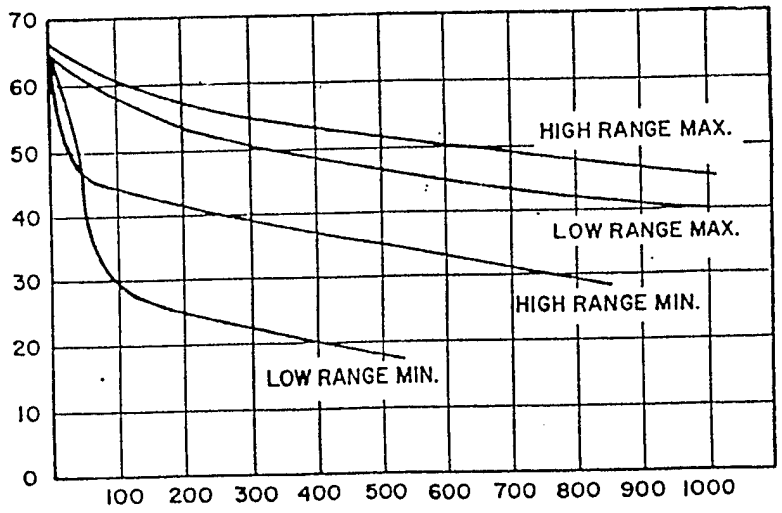

Figure 35. Volt-Ampere characteristics of L-TEC welding power supply.

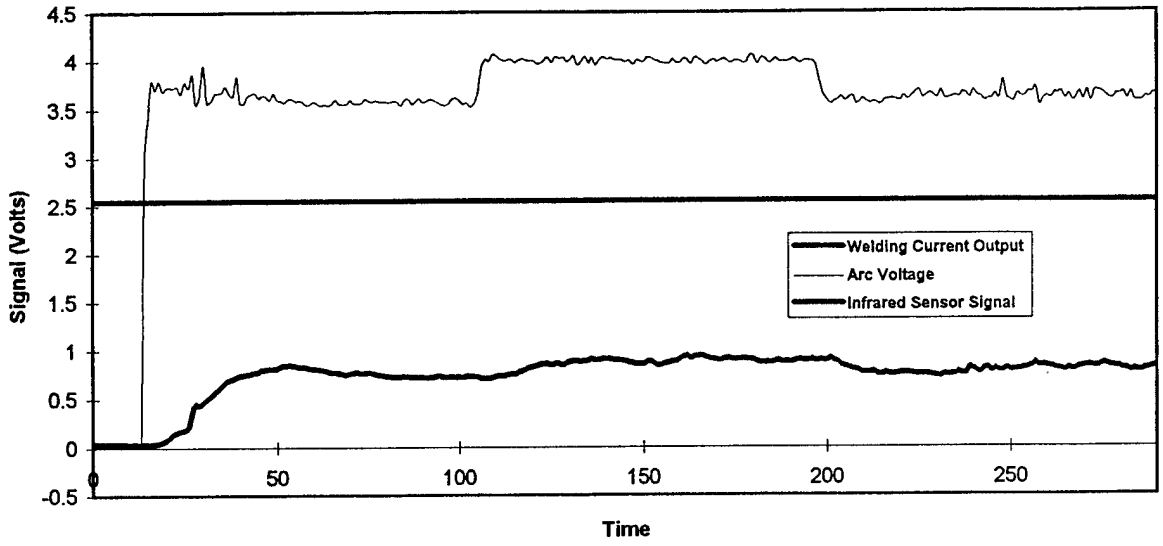

Figure 36. Graph showing the change in the IR sensor signal due to the change in the arc voltage.

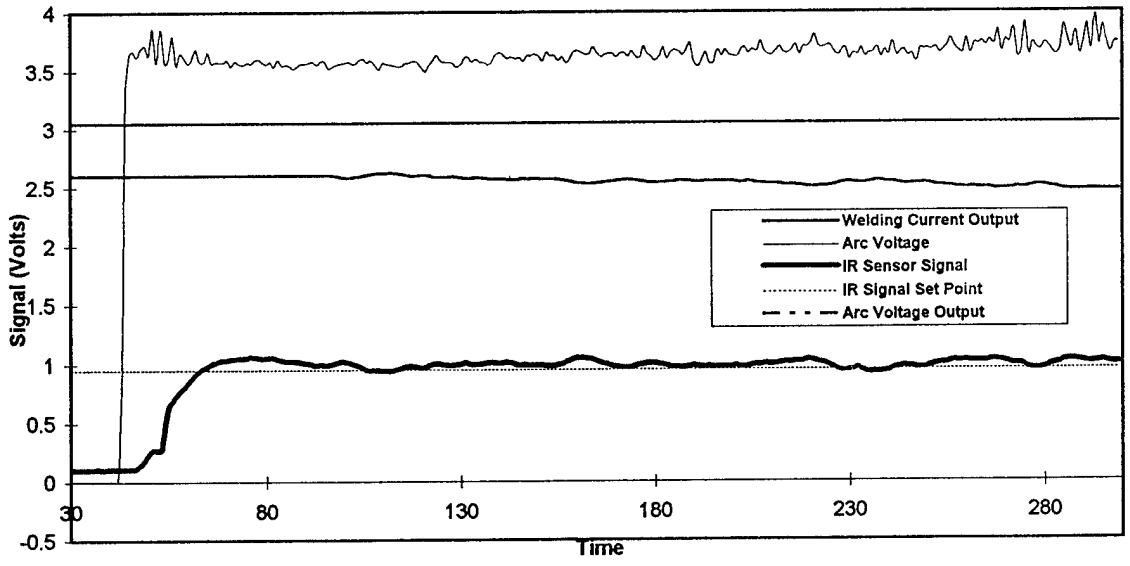

Figure 37. Graph showing the increase in the arc voltage due to the decrease in the welding current.

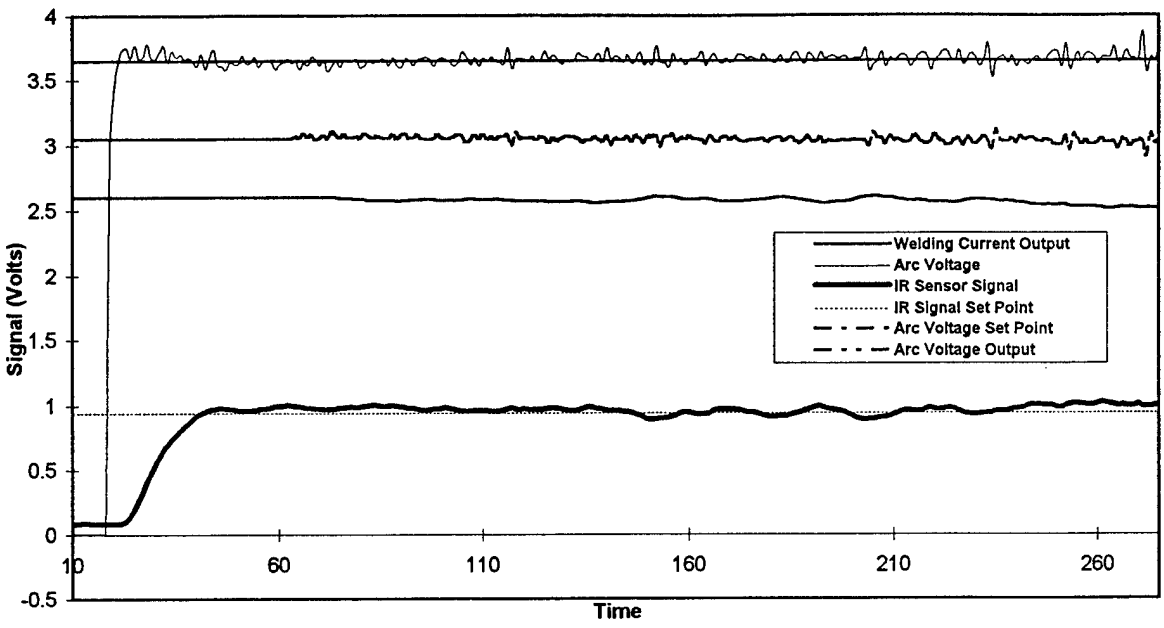

Figure 38. Graph showing the IR sensor signal, arc voltage, welding current output, IR signal set point, arc voltage set point and the arc voltage output for a bead-on-plate weld performed with both automatic welding current and arc voltage control

V.CONCLUSIONS

The theoretical and experimental investigation of infrared thermal sensing associated with the arc welding processes for weld quality control applications has led to the following conclusions.

- One type of point infrared sensor was developed in this study. The developed point infrared sensor system appears to offer a practical and convenient method for measuring and control of submerged arc welding processes. The point sensing method appears to be a promising alternative to line-scan and area-scan methods.
- A point infrared sensor was designed and developed based on a thermopile detector. The sensor was small and unobtrusive so that the detector could be placed within 20 mm of the arc center. The sensor was cooled to maintain a constant detector temperature, which ensured its operational integrity near the harsh welding arc.
- Theoretical study shows that perturbations, such at thickness changes, existence of stiffeners, and joint gap variations, change the temperature distribution on the plate surface. By monitoring the temperature distributions on the plate surface, real time quality control can be applied.
- Experimental results show that point infrared sensor can detect the temperature changes caused by the changes of thickness, existence of stiffener, and gap variations in real time. The temperature of the sensing point can be maintained at the setpoint by using a PID control algorithm. The quality and reliability of the welds produced can be significantly improved.

REFERENCES

1. Hardt, D.E. and J.M. Katz, "Ultrasonic measurement of weld penetration", *Welding Journal* 63 (9) (1984), pp.273s - 281s.

2. Carlson, N.M. and J.A. Johnson, "Ultrasonic sensing of weld pool penetration", *Welding Journal* 67 (11) (1988), pp.239s - 246s.

3. Carlson, N.M. and J.A. Johnson, "Control of GMAW: Detection of discontinuities in the weld pool", *Welding Journal* 69 (7) (1990), pp.256s - 263s.

4. Carlson, N.M., J.A. Johnson and E.D. Larsen, "Non-contacting ultrasonic system for defect detection in solidified weld metal", in *Review of Progress in Quantitative Non-Destructive Evaluation*, Vol 12A, Plenum Press, pp.949 - 956.

5. Fenn, R., "Ultrasonic monitoring and control during arc welding", *Welding Journal*, 64 (9) (1985), pp.8 - 22.

6. Zackenhouse, M. and D.E. Hardt, "Weld pool impedance identification for size measurement and control", ASME *Journal of Dynamic Systems, Measurement and Control*, 105 (3) (1983), pp.179 - 184.

7. Renwick, R.J. and R.W. Richardson, "Experimental investigation of GTA weld pool oscillations", *Welding Journal*, 62 (2) (1983), pp.29s - 35s.

8. Xiao, Y.H. and G. den Ouden, "Weld pool oscillations during GTA welding of mild steel", *Welding Journal*, 72 (8) (1993), pp.428s-434s.

9. Madigan, F.B., R.J. Renwick, D.F. Farson and R.W. Richardson, "Computer control of full penetration GTA welds using pool oscillation sensing", in *Proc. 1st Conference on Computer Technology in Welding*, TWI, London, (1986), pp.165 - 174.

10. Smith, C.J., "Self adaptive control of penetration in tungsten inert gas weld", in *Advances in Welding Processes*, ed. J.C. Needham, The Welding Institute, Cambridge, pp.272 - 277.

11. Kovacevic, R., Y.M. Zhang and L. Li, "Monitoring of weld joint penetration based on weld pool geometrical appearance", *Welding Journal*, 75 (10) (1996), pp.317s - 329s.

12. Richardson, R.W., D.A. Gutow, R.A. Anderson and D.F. Farson, "Coaxial arc weld pool viewing for process monitoring and control", *Welding Journal*, 63 (3) (1984), pp.43 - 50.

13. Rokhlin, S.I. and A.C. Guu, "Computerized radiographic sensing and control of arc welding process", *Welding Journal*, 69 (3) (1990), pp. 83s - 97s.

14. Doeblin, E.O., "Measurement Systems - Application and Design", McGraw Hill, New York, (1975), pp.540 -544.

15. Chin, B.A., N.H. Madsen and J.S. Goodling, "Infrared thermography for sensing the arc welding process", *Welding Journal*, 62 (9) (1983), pp.227s - 234s.

16. Nagarajan, S., W.H. Chen and B.A. Chin, "Infrared sensing for adaptive arc welding", *Welding Journal*, 68 (11) (1989), pp.462s - 466s.

17. Wang, Y., and B.A. Chin, "On-line sensing of weld penetration using infrared thermography", in *Optical Techniques for Industrial Inspection*, Proc. SPIE 665, (1986), pp.314 - 320.

18. Banerjee, P., S. Govardhan, H.C. Wikle, J.Y. Liu and B.A. Chin, "Infrared sensing for on-line weld process monitoring and control", in *Manufacturing Science and Engineering*, editor K.F. Ehmann, (1993), pp. 907 - 918. New York:ASME.

19. Doumanidis, C.C. and D.E. Hardt, "Simultaneous in-process control of heat affected zone and cooling rate during arc welding", *Welding Journal*, 69 (5) (1990), pp.186s - 196s.

20. Brown, B., "The measurement and monitoring of resistance spot welds using infrared thermography", in *International Conference on Thermal Infrared Sensing for Diagnostic and Control*, Proc. SPIE 581, (1986), Cambridge, MA.

21. Ramsey, P.W., J.J. Chyle, J.N. Kuhr, P.S. Myers, M. Weiss and W. Groth, "Infrared temperature sensing systems for automatic fusion welding", *Welding Journal*, 42 (8) (1963), pp.337s - 346s.

22. Wikle, H.C., Ph.D., Dissertation (1998)

23. Kottilingam, S.C., H.C. Wikle and B.A. Chin, "Real-time monitoring and control of submerged arc welding process using infrared sensors", in *5th International Conference in Trends in Welding Research*, July, (1998).

24. Seigel, R. and J.R. Howell, "Thermal Radiation Heat Transfer", Washington Hemisphere Publishing (1981).